 doi:10.20944/preprints202207.0158.v1

Article

Evaluation of Surface Water Resource Availability under the Impact of Climate Change in the Dhidhessa Sub-Basin, Ethiopia

Damtew Degefe Merga[1,*], Dereje Adeba [1], Motuma Shiferaw Regasa [2], Megersa Kebede Leta [3,*]

[1] Department of Hydraulic and Water Resources Engineering, Institute of Engineering and Technology, Wollega University, 395 Nekemte, Oromia Region, Ethiopia; mo_dereje2018@yahoo.com
[2] Department of Hydrology and Hydrodynamics, Institute of Geophysics, Polish Academy of Sciences, 01-452 Warsaw, Poland; mregasa@igf.edu.pl
[3] Faculty of Agriculture and Environmental Sciences, University of Rostock, Satower Str. 48, 18051 Rostock, Germany
* Correspondence: hwre2020@gmail.com or afaankooni@gmail.com (D.D.); megersa.kebede@uni-rostock.de (M.K.L.)

Abstract: The main target of this study was to evaluate the impact of future climate change on the available surface water resources in the Dhidhessa Sub-basin, Abbay Basin, Ethiopia. For the prediction, high-resolution Regional Climate Models (RCMs) from multiple climate models with data from Representative Concentration Pathways (RCPs) prepared by the CCAFS were used. The predictions of future discharge (stream flow) were based on climate scenarios data of baseline period of 1991 to 2020 and for the future with two time windows, 2044 (2030–2059) and 2084 (2070–2099), on a monthly time step after bias correction was conducted to both precipitation and temperature in the future climate under each RCP scenario. After sensitivity analysis, calibration (1994–2011), and validation (2012–2020) of the model for the Dhidhessa Sub-basin with the SUFI-2 program in the SWAT-CUP model, the SWAT model was used to determine water balance and stream flow from the SWAT model system. The SWAT model performed well in predicting stream flow in the Dhidhessa Sub-basins, with a coefficient of determination (R^2) ranging from 0.8 to 0.94 and a Nash Sutcliffe value (NSE) ranging from 0.76 to 0.89. The percent decrease in mean annual stream flow from 2044 and 2084 were 10 %, in 2044, and 6.3% in 2084 respectively. The seasonal result under short-term 2044 of stream flow present change significantly decreased in spring, winter, and autumn with 20.2%, 67.4%, and 67.4% respectively. While summer season increased by 43.1%, under short-term 204. In long-term 2084 percent change declined except summer seasons, with 14.7%, 58.1%, and 3.3%, change in spring, winter, and autumn, respectively, and summer, with 51.1% increased and With RCP4.5 (1.64%) and RCP8.5 (2.1%) changed. In the future Dhidhessa stream flow increases and decreases from the baseline era. The decreasing stream flow in 2044 and 2084 will negatively affect agricultural production. This study revealed that any effect on this river resulting in a drop in flow will have a direct impact on ongoing water resource development and socio-economic development of the area.

Keywords: Dhidhessa; Sub-basin; RCP; stream flow; SWAT; Climate Models; Surface Water Availability; Scenario

1. Introduction

Global warming is defined as any long-term, systematic, statistically significant change in climate, such as changes in precipitation and temperature, which last for years or longer. As a result, changes in extreme weather events and long-term rainfall or temperature patterns can be indicators of climate change. Long-term climate (bases usually occur at 30-year intervals) [1]. Climate change is one of the greatest challenges of the twenty-first century and is widely recognized as one of the most serious issues of the century. Climate change is now widely accepted as a possibility, and some changes are needed; over the past 100 years, temperatures have increased by 0.74°c (between 1906 and

 doi:10.20944/preprints202207.0158.v1

2005) [1]. This happened in two stages from 1910 to 1940 and is still potent from the 1970s to the present [2]. According to the IPCC Scientific Assessment Report, global temperatures are likely to rise by 1.4°c to 5.8°c between 1990 and 2100 [3,4]. As the air temperature rises, so does the water temperature. As water temperatures rise, water pollution is becoming more of a problem, and more aquatic habitats will be adversely affected [1]. In the 20th century, global oceans rose 12-22cm, causing the ice and ice cap to melt (both shrunk in size on both sides [5].The IPCC notes that the extent also changed , intensity, frequency, and types of precipitation throughout the last century have been observed in [5].Climate affects the availability of water resources especially rainfall, has a significant effect on the frequency of waterfalls through the hydrological cycle and, consequently, the quantity of water available .

Just as there is abundant rainfall, there is also abundant water. Drought and low rainfall limit the availability of water resources by the same mechanism [6]. Temperature affects the availability of water resources [7]. The impacts of climate change on meteorology, hydrology and ecology, in addition to their economic and social importance, are critical factors in water resource management, agriculture and ecosystems across the country. According to [3], access to water resources responds to global warming in ways that can adversely affect water supplies. Climate change was often measured in terms of key weather variables, such as air temperature and precipitation [4]. The Global Climate Change Model (GCM) predicts future climate change global warming [4,8]. The greenhouse effect is an important natural way of life on earth, but human activity has changed the balance in this machine [9]. Climate change directly affects the value and quality of water resources. Changes in temperature and precipitation due to climate change are predicted to affect water supplies locally and temporally [9]. Hydrological cycles can persist in ecosystems despite human impacts and climate change [10]. Anthropogenic stimuli such as rapidly increasing deforestation and freshwater withdrawals can alter rainfall and temperature patterns resulting in limited water resource conflicts [6]. Under changing land use and land cover and climate, proper integration of water resources and water resource sharing among different water users are major problems that different civilizations are currently facing or will face in the future as a result of these practices [11].

This study addresses the effects of climate change on the flow hydrology and surface water availability. The Dhidhessa sub-basin is one of the major sources of the Blue Nile and is considered the most important tributary of its discharge contribution. It is located in the southwestern part of the upper Blue Nile basin [12]. The Dhidhessa River rises in the Gomma and Gumaa mountain ranges and flows through the major rivers of the Jimma, Illubabor, and Wollega regions. In Jimma Arjoo district, Dhidhessa sub-watershed was selected as one of the Blue River watersheds because it is planned to conduct various multi-purpose water resource development projects and assess the overall impact. Determination of available surface water resources in the context of climate change is important for evaluating the sustainability of the project and potentially appropriate mitigation measures.

In this study, a semi-distributed water assessment (SWAT) model with an efficient parameter was used to generate precipitation and temperature climate change scenarios. It is important to evaluate the availability of surface water resources under climate change impacts, as it allows for better forecasting, and provides for the development of climate change mitigation and adaptation measures in response to climate change. Furthermore, this study can raise awareness on future risks of climate change impacts on water resource availability. Using hydrological modeling, including Water Assessment System (SWAT), regional climate model, and GIS software, this study was conducted to investigate the impact effects of climate change on water resource availability in Dhidhessa sub-basin.

2. Materials and Methods

2.1. Study Area Description

Preprints (www.preprints.org) | NOT PEER-REVIEWED | Posted: 11 July 2022 doi:10.20944/preprints202207.0158.v1

In western Ethiopia, the Dhidhessa Sub-basin originated from the Abbay Basin in the southwestern region as shown in (Figure 1). The study area lies between 08°00′00″and 09°00′00″north latitude and 35°00′00″and 37°00′00″east longitude. The sub-basin occupies an area of about 19,629.83km[2]. Flat-sloped valley terrain characterizes the lower part of the Dhidhessa Sub-basin, which is rocky, very rugged, and has steep slope topography. The analysis will include key water resource development projects and sites of interest, as well as distribution through the main stream of the Dhidhessa River and four major rivers, namely Dambi (Agaroo), Dabena near Buno Bedele, Wama, and Dhidhessa near the Arjoo River.

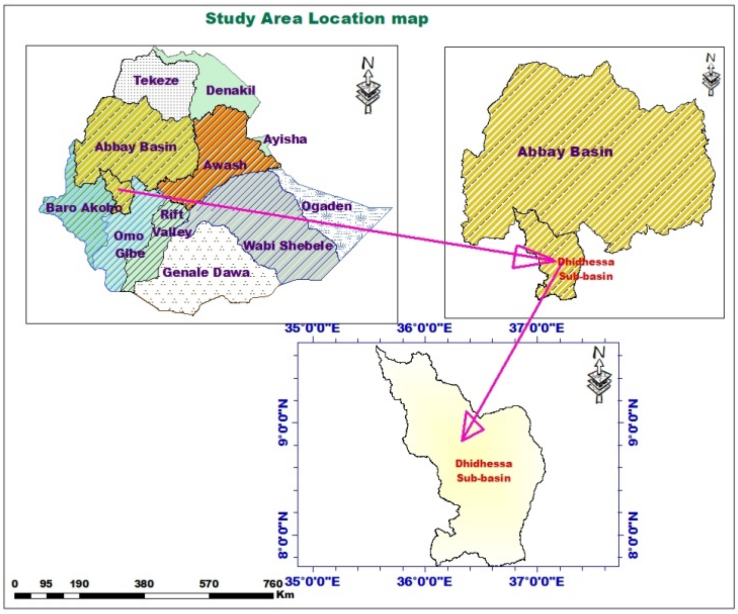

Figure 1. Location map of Dhidhessa Sub-basin

The elevation of the study area is between 818meter a.m.s.l. to 3146meter a.m.s.l as shows (Figure 2). The watershed mainly covers the Kola and Weina dega climate zones, according to the Ethiopian climate classification based on elevation (i.e. < 500m: Bereha, 500-1500/1800: Kola, 1500/1800 - 2300/2000). 2400: Weina dega, 2300/2400-3200 : Dega, and >3200: Wurch [13].

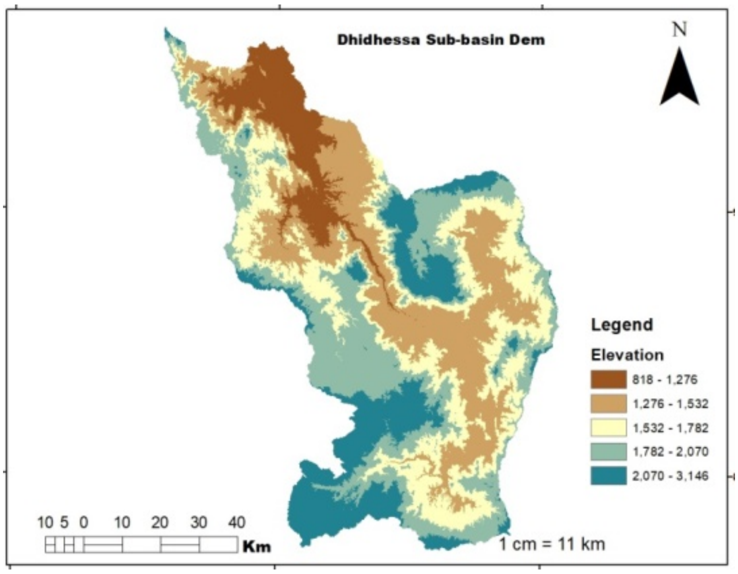

Figure 2. Topography of Dhidhessa Sub-basin

The Dhidhessa sub-watershed is the largest of the Upper Blue Nile rivers in terms of water volume, contributing approximately a quarter of the total discharge as recorded at the Ethiopia-Sudan border alone [14]. Dabana near Bunoo Bedele, Dambi (Agaroo), Dhidhessa near Arjoo, and Wama are the major catchment areas of the discharge of the Dhidhessa basin (Figure 3) indicating a rise in stream discharge. The Wama River enters the Dhidhessa River from the north-east, with a watershed of about 3767km², the Dabana flows from west to east, then north, near Bunoo Bedele, until it joins the Wama River. The Dabana sub-catchment near Bunoo Bedele is estimated to be around 4842 km². Figure (3) shows the statistical analysis of observed stream data from 1991 to 2020 showing the maximum peak flow Record in August.

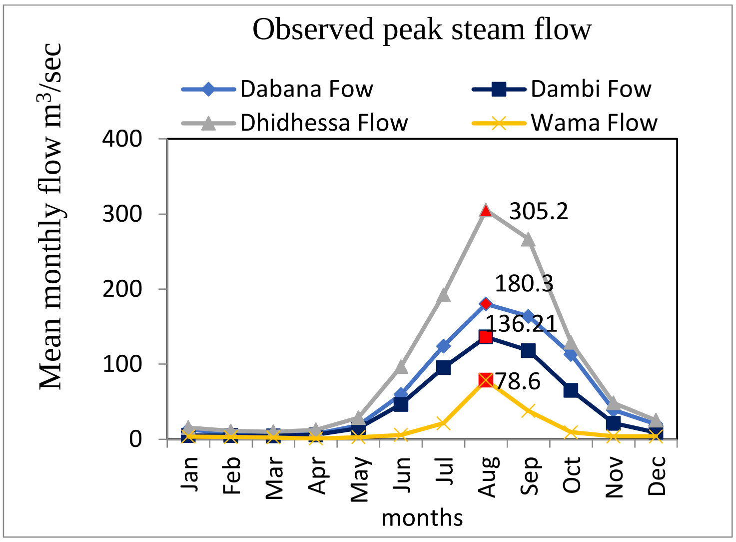

Figure 3. Peak Steam Flow of Catchments

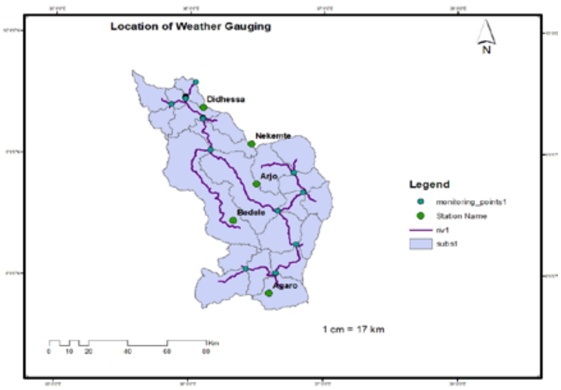

Figure 4. Location of Gaging Stations

The Dhidhessa catchment was delineated using a digital elevation model (DEM) with a resolution of 20m x 20m from the GIS Division of the Ministry of Water, Irrigation, and Energy (MoWIE). All LULC maps and data sets were collected in shape file format from the GIS Department of the Ministry of Water, Irrigation, and Energy (MoWIE). For the SWAT database/map window, the land use map was reclassified to display land use based on specific LULC types and corresponding crop parameters. To associate SWAT class grid values with LULC, a view was created from the map window database that defines the SWAT land use code for each LULC type.

Land use classes in the study area are Agricultural Land: Generic (AGRL), Agricultural-Row-Cropland (AGRR), Banana (BANA), Coffee (COFF), Forest-Deciduous-Leafy (FRSD), Forest-Evergreen (FRSE), Mixed Forest (FRST), Pasture (PAST), Range-Grasses

 doi:10.20944/preprints202207.0158.v1

(RNGE), Urban (URBN), Wetland-Forest (WETF), Wetland-Mixed (WETL), and Wetland-Forest Not Having (WETN). Agricultural Land: The generic covers a large area within this land use classification as indicated by (Figure 4). The FAO/Globe soil classification system is used to classify consumer soils from the map window database in the study sub-basin. Soil types Sub-basin sedimentation

The major soil types considered in the study area include sub-basin sedimentation Cambisols, district Cambisols, eutric leptosols, eutric leptosols, eutric regosols, eutric vertisols, haplic acrysols, haplic alisols, haplic nitosols, and rhodic nitosols were considered in the study, according to the FAO. (Figure 4) shows that Haplic Alisols are the most abundant soils in the study area and covered the area of the sub-basin.

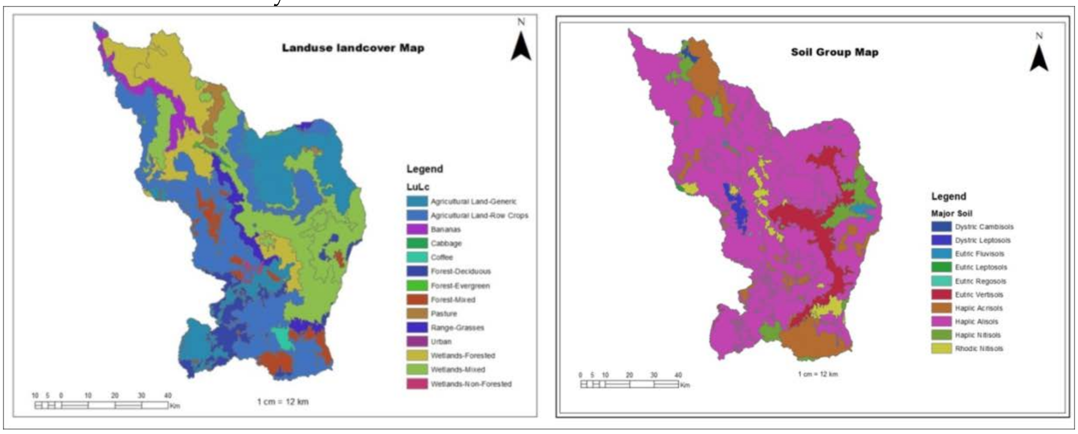

Figure 5. Land use/Land Cover and soil map

2.2. Methodology

2.2.1. Data Collection and Use

a. Meteorological, Hydrological, and Topographical Data

Precipitation, maximum and minimum temperature, relative humidity, wind speed, and solar radiation at five representative stations in the sub basin (Agaroo, Arjoo, Bedele, Dhidhessa, and Nekemte) were observed daily continuously meteorological data were collected for a period of 30 years (1991-2020) from the National Meteorological Agency of Ethiopia (NMAE). The CORDEX Africa dataset is a database of future climate data for the years 2010 to 2099. CORDEX models were used to simulate monthly precipitation, min and max temperature from http://www.ccafs-climate.org/data_spatial_down_scaling/. stream flow data were collected from the Dhidhessa rain gauge stations (1991-2020) and GIS databases of the Ministry of Water, Irrigation, & Energy of Ethiopia (MoWIEE) Hydrology and GIS Department, respectively, for surface water evaluation in the basin.

Table 1. Listed Weather Monitoring Stations

Station Name	Zone	Station Elevation	Latitude	Longitude	Data coverage	% of missing Rainfall	% of missing Temp.(°c)
Agaro	Jimma	1666	7.85	36.6	1991-2020	22	22.5
Arjo	East wollega	2565	8.75	36.5	1991-2020	21	37.5
Bedele	Illubabor	2011	8.45	36.33	1991-2020	21	17.5
Didhessa	East wollega	1310	9.38	36.1	1991-2020	20	46
Nekemte	East wollega	2080	9.08	36.46	1991-2020	21	20.5

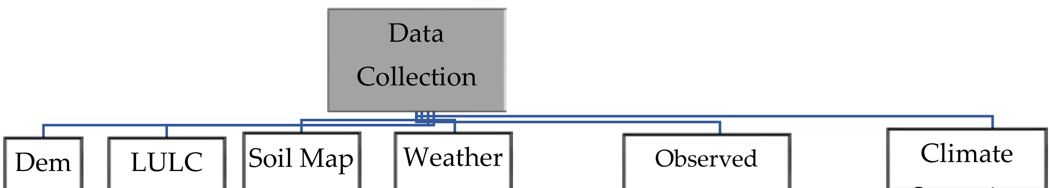

Figure 6. Research Methodology Flow Chart

Soil and Water Assessment Tool (SWAT) simulations were used to assess surface water availability. It is a semi-distributed model that can be used to simulate the effects of climate change on stream flow and many other presences at the small-water scale. Specific input data, such as climate, hydrology, and spatial data need to be used. Spatial data were processed using GIS Tools, which provided an interface to the SWAT model as both. GIS version 10.3 and SWAT 2012 were used in this study. Stochastic Uncertain Fitted, Version 2 (SUFI-2) is a parameter and model uncertainty analysis program integrated with the standalone program SWAT Calibration and Error Tool (SWAT-CUP).

2.3. Basin Future Climate Change Scenario and the selected model

Each model does have its advantages and disadvantages [15]. The performance of each model used in the study was compared to observation to attain this specific objective. The performance of an ensemble of models was also computed and compared to the models performance versus the observation. This study used climate data from high-resolution regional climate models from the CORDEX-Africa database. The driving model or GCMs are chosen based on earlier research or study conducted in the Dhidhessa River sub-basin [16,17,18]. As a result, the (Danish Hydrologic Institute) DMI-HIRHAM5, (Regional Atmospheric Climate Model Version 2.2) KNMI-RACMO22T, and (Swedish Meteorological and Hydrological Institute) SMHI-RCA4 driving models were chosen, and downscaling was performed using the most recent version of the regional climate model. Some of the World Meteorological Organization's (WMO) standard statistical metrics were used to compare model outputs to observations [19]. These statistics include bias, root mean square error, and coefficient of variation [19].

$$Bias = \frac{1}{N}\sum\nolimits_{i=1}^{N}(P_i - Obs_i)$$

Preprints (www.preprints.org) | NOT PEER-REVIEWED | Posted: 11 July 2022 doi:10.20944/preprints202207.0158.v1

$$RMSE = \sqrt{\frac{1}{N}\sum_{i=1}^{N}(P_i - Obs_i)^2}$$

$$CV = \frac{\sum_{i=1}^{N}(P_i - \bar{P})(Obs_i - \overline{Obs})}{\left(\sqrt{\frac{1}{N}\sum_{i=1}^{N}(Obs_i - \overline{Obs})^2}\right)\left(\sqrt{\frac{1}{N}\sum_{i=1}^{N}(P_i - \bar{P})^2}\right)}$$

The simulated and measured values are P and Obs, respectively, while the simulated and observed pairs are i and N.

2.3.1. Bias Correction

RCM models often show [20] significant biases when evaluated to observed data, even local downscaling to high resolution. Since these biases of rainfall and temperature were observed to vary spatially [21], bias corrections were performed for each sub-basin separately [21]. Temperature and rainfall data from climate models were bias-corrected at the sub-basin level in this study. The linear shifting and scaling method have been used to bias-correct the min and max temperatures by (Equation 1) [14].

$$T_{Corrected} = T_{mean\ Obs} + \frac{\delta(T_{Obs})}{\delta(T_{RCM})}(T_{RCM} - T_{mean\ Obs}) + (T_{mean\ Obs} - T_{mean\ RCM}) \quad (1)$$

Where: $T_{Corrected}$ is the corrected daily temperature; $T_{(mean\ Obs)}$ is the mean observed temperature; and $T_{(mean\ RCM)}$ is the mean simulated temperature; T_{RCM} is the uncorrected daily temperature from the RCM model; T_{Obs} is the observed daily temperature; $T_{(mean\ Obs)}$) is the mean observed temperature, and $T_{(mean\ RCM)}$ is the mean simulated temperature. The modification was done separately to data from each of the twelve months [14].

A power transformation was used, which corrects both the coefficient of variation and the mean ([22]. Every daily rainfall quantity P is changed into a corrected P* using (Equation 2) the following nonlinear correction:

$$P^* = ap^b \quad (2)$$

Where is the variable's corrected value (rainfall), "b" is the scaling exponent, which is generated iteratively, and the RCM precipitation time series' coefficient of variation equals that of the observed precipitation time series. After that, the constant "a" is determined to ensure that the mean of translated precipitation values equals the observed mean.

$$b = \frac{\delta_{P\ obs_{day}}}{\mu_{P_{obs\ day}}} - \frac{\delta_{PRCM_{day}}}{\mu_{PRCM_{day}}},\ P^+ = (P_{RCM\ day})^b,\ a = \frac{\mu_{P\ obs_{day}}}{\mu_{P^+_{RCM\ day}}},\ and\ P^* = (aP^+)^b$$

δ= standard deviation, μ = mean of the rainfall (RF), P^+= corrected rainfall (RF), P_{RCM}= Uncorrected rainfall (RF), $P\ obs$= Observed rainfall (RF), and P^*=Biasd rainfall (RF)

2.4. Hydrological Component of the SWAT Model

The hydrological component of the SWAT model is based on the water balance equation. Soil water, surface runoff, intercept, daily precipitation, evapotranspiration, percolation, lateral groundwater flow, return flow or base flow, snowmelt, transmission losses, and water production they are all part of the SWAT model. Discharge from the vadose zone to deep water and base flow to and from deep water channels or base flow are the only factors considered for the hydrological model in SWAT. Groundwater from the deeper aquifer is not taken into account, because water reaching the deeper aquifer is assumed to contribute to stream flow at locations outside the reservoir. According to [23], surface runoff, lateral flow from the soil profile, and return flow or base flow from the

Preprints (www.preprints.org) | NOT PEER-REVIEWED | Posted: 11 July 2022 doi:10.20944/preprints202207.0158.v1

deep aquifer all contribute to the water in the stream. Water discharged into shallow aquifers is considered lost from the watershed system and is therefore not included in the water assessment [24]. The soil water content of the catchment is calculated using (Equation 3) below:

$$S_{Wt} = S_{Wo} + \sum_{i=1}^{t}\{R_{day} - Q_{Surf} - E_a - W_{Seep} - Q_{gw}\}i \tag{3}$$

Where S_{Wt} is the final soil water content (mm). S_{Wo} is the initial soil water content on day i (mm). t is the time (days). R_{day} is the amount of precipitation on day i (mm). Q_{surf} is the amount of surface runoff on day i (mm). E_a is the amount of evapotranspiration on day i (mm). W_{seep} is the amount of water entering the vadose zone from the soil profile on day i (mm); and Q_{gw} is the amount of return flow on day i (mm). The water balance components in the SWAT model are calculated from the hydrological cycle and the equilibrium period/warm-up period using SWAT input time series temporal and spatial data as follows.

2.4.1. Surface Runoff

SWAT simulates surface runoff volumes and peak runoff rates for each HRU using daily or sub-daily rainfall amounts. The SCS curve number approach and the Green & Ampt infiltration method are two SWAT methods for evaluating surface runoff volume. The latter technique is more accurate in evaluating runoff volume, but it requires sub-daily time step data, which makes it nearly impossible to utilize in our nation. As a result, the SCS curve numbering approach was used. The general (Equation 4) for the SCS curve number method:

$$\mathrm{Q_{Surf}} = \frac{(\mathrm{R_{day}} - \mathrm{I_a})^2}{(\mathrm{R_{day}} - \mathrm{I_a} + \mathrm{S})} \tag{4}$$

Where, Q_{surf} is the accumulated runoff or rainfall excess (mm), R_{day} is the rainfall depth for the day (mm water), I_a is initial abstraction which includes surface storage, interception and infiltration prior to runoff (mm water), and S is retention parameter (mm water). The retention parameter S can be calculated by using (Equation 5).

$$\mathrm{S} = 25.4 * \left(\frac{1000}{\mathrm{CN}} - 10\right) \tag{5}$$

Where, CN is the curve number for the day and its value is the function of land use practice, soil permeability and soil hydrologic group. The initial abstraction, I_a, is commonly approximated as 0.2S and (Equation 6) becomes:

$$\mathrm{Q_{Surf}} = \frac{(\mathrm{R_{day}} - 0.2\mathrm{S})^2}{\mathrm{R_{day}} + 0.8\mathrm{S}} \tag{6}$$

2.4.2. Peak Discharge

The peak volume flow rate past a specific location during a storm event is known as the peak discharge or peak surface runoff rate. The peak run-off rate is used to estimate sediment loss and water quality and is a measure of a storm's erosive force. SWAT uses a modified rational method to compute the peak runoff rate (see Equation 7) [24].

$$\mathrm{Q_{peak}} = \frac{\mathrm{CiA_{total}}}{3.6} \tag{7}$$

Where: Q_{peak} is peak runoff rate (m^3/s),
C is the runoff coefficient,
i is the rainfall intensity (mm/hr.),
Sub-basin area (km2) and 3.6 is conversion factor.

2.4.3. Water Yield

Preprints (www.preprints.org) | NOT PEER-REVIEWED | Posted: 11 July 2022 doi:10.20944/preprints202207.0158.v1

After the water balance system has been satisfied, the remaining total amount of water leaves each HRU and sub basin and enters the main channel stream flow. SWAT calculates the total water yield contributes to stream flow in the reach as the net water passes through the HRU and sub basin using the following equation:

$$\mathrm{WYID} = \mathrm{SURQ} + \mathrm{LATQ} + \mathrm{GWQ} - \mathrm{TLOSS} \tag{8}$$

where: WYLD= water yield (mm) is the net amount of water leaves HRU and sub basin and contributes to main channel stream flow, SURQ= surface runoff contribution to stream flow, LATQ= lateral flow contribution to stream flow (mm), GWQ= groundwater (base flow) from the shallow aquifer that enters the main channel (mm). TLOSS is a transmission loss (water lost from tributary channels and main channel bed loss (mm).

2.5. Evaluation of the SWAT Model Performance

For various simulations, performance data was used to evaluate whether calibration and validation periods, spatial and temporal ranges, and specific performance Evaluation of Calibrations were needed [25]. Calibration is a combination of manual and automated processes that evaluate parameters of the model that cannot be directly measured. The validation process looks to see if the model is working appropriately, and provides a framework for model calibration and validation that is systematic. The author explains how to calibrate the SWAT model [26]. From 1991-2020, the model was in use for 30 years, from 1994 to 2011, the watershed's calibration was carried out. Validation of the watershed was also completed for the years from 2012 to 2020. A model must fulfill all three of the following criteria to be considered for the chosen ensemble [27]**.** Three criteria were used in this study: the coefficient of determination (R^2), the Nash-Sutcliffe Index (NSE), and the percent bias (P_{BIAS}).

2.5.1. Coefficient of Determination (R^2)

The coefficient of determination (R^2) is a measure of how much variance in derived data the model experiences. The coefficient of determination (R^2) is the most generally used parameter for evaluating a model's performance, as seen in the following (Equation 9):

$$R^2 = \left\{ \frac{\sum_{i=1}^{n} (O_i - O_{mean})(P_i - P_{mean})}{\sqrt{\sum_{i=1}^{n} (O_i - O_{mean})^2} \sqrt{\sum_{i=1}^{n} (P_i - P_{mean})^2}} \right\} \tag{9}$$

Where O_i denotes observed flow discharge at the time i,
O_{mean} denotes average observed flow discharge,
P_i denotes simulated flow discharge at the time i,
P_{mean} denotes average simulated flow discharge, and n is the number of flow discharge data recorded. The (Table 2) shows the performance rating R^2 criteria defined by [28] for SWAT model calibration and validation.

R^2 provides the strength of relation between observed and simulated values. Its value ranges from 0 to 1, a value close to 0 means very low correlation whereas a value close to 1 represents high correlation between observed and simulated discharge.

2.5.2. Simulation Coefficient of Nash Sutcliffe (NSE)

The Nash-Sutcliffe simulation coefficient (N_{SE}) measures how well the observed versus simulated data plot fits the 1:1 line. A formula used to determine N_{SE} is shown in (Equation 10).

$$\mathrm{NSE} = 1 - \frac{\sum_{i=1}^{n} (O_i - P_i)^2}{\sum_{i=1}^{n} (O_i - O_{mean})^2} \tag{10}$$

Because of the classification, performance ratings for the N_{SE} of this model are evaluated on multiple levels shows by (Table 2) [28]. N_{SE} determines the relative magnitude of the residual variance compared to the measured data. Its value ranges from -∞ to 1, where

1 indicates a perfect model and a value less than 0 indicates that the mean value of the observed time series would have been a better predictor than the model.

2.5.3. Percentage Bias (PBIAS)

PBIAS (percentage bias) determines whether the simulated data is larger or smaller than the observed data [28]. PBIAS results of (Table 2) shows that the model simulation is correct ranges. Positive values show an underestimation of bias by the model, although negative values indicate over evaluation of bias by the model [28]. A formula used to determine PBIAS is shown in (Equation 11):

$$\mathrm{PBIAS} = \frac{\sum_{i=1}^{n}(O_i - P_i)}{\sum_{i=1}^{n} O_i} * 100 \tag{11}$$

For the evaluation of models, [29] assigned values of ENS, PBIAS, and R² as the following (Tables 2) shows. It measures the difference between the simulated and observed quantity and its optimum value is 0. A positive value of the model represents underestimation whereas a negative value represents the model overestimation.

Table 2. Classification of Indices under the Calibration and Validation models

NES	PBIAS	R^2	Classification
0.75 < NES ≤ 1	PBIAS ≤ ±10	0.75 < R2 ≤ 1	Very good
0.6 < NES ≤ 0.75	±10 ≤ PBIAS ≤ ±15	0.6 < R2 ≤ 0.75	good
0.36 < NES ≤ 0.6	±15 ≤ PBIAS ≤ ±25	0.5 < R2 ≤ 0.6	satisfactory
0.00 < NES ≤ 0.36	±25 ≤ PBIAS ≤ ±50	0.25< R2 ≤ 0.5	Bad
NES ≤ 0.00	±50 ≤ PBIAS	R2 ≤ 0.25	Inappropriate

3. Result and Discussions

3.1. Hydro-Meteorological Database Results.

3.1.1. Test Analysis of Rainfall Trends in the Study Area.

The Mann-Kendall trend test was used to evaluate for trends in precipitation and temperature data (Fentaw et al., 2019). A test the null hypothesis that there is no trend in the data series, while the alternative hypothesis states that there is a trend in the time series. Mann-Kendall procedure tests were performed in XLSTAT (2015). Kendall's Mann-test seems to be a non-parametric method [30] that tests trends in time series without specifying linear or nonlinear trends [31], and is less susceptible to outliers [32]. The MK test has been widely used to identify important trends in hydro-meteorological time series data, and is usually promoted mainly by the World Meteorological Organization (WMO) [33]. The test was performed with a 5% significance gate. In test interpretation, the p-value and Sen's slope were the two most important variables. Such Mann-Kendall test statistics [34].

The Mann–Kendall test is a widely used nonparametric test for determining whether time series data have monotonic behavior [35]. The observed annual series of precipitation, temperature, and stream discharge of the Dhidhessa sub-basin were evaluated using the non-parametric Kendall trend test with 5 percent significance level. The significance test in this study used a normalized P-value. When the P-value is small at the 0.05 alpha significance level, the null hypothesis should be rejected, and the hypothesis accepted, vice versa. Figure 8 shows the peak trend for Arjoo, Bedele, Dhidhessa, and Nekemte rainfall stations, but the worst trend for Agaroo. As indicated in (Table 3), the rate of change of annual precipitation is highest at Arjo station (2.2), and lowest at Agaroo station (2.0).

Preprints (www.preprints.org) | NOT PEER-REVIEWED | Posted: 11 July 2022 doi:10.20944/preprints202207.0158.v1

(Table 3) shows the estimated sens slope and Mann-Kendall trend test for rainfall for each site (Figure 7) and shows the mean values for all Dhidhessa sub-catchment stations, the sen slope value, and the z value for rainfall.

Table 3. Sens Slope Estimations and Mann-Kendall Trend Test for Rainfall

RF(1991-2020)										
Month	Agaroo		Arjoo		Bedele		Dhidhessa		Nekemte	
	Sen's slope	Z-Value	Sen's slope	Z-Value	Sen's slope	Z-Value	Sen's slope	Z-Value	Sen's slope	Z-Value
Jan	-1.0	-2.7	2.3	0.9	1.8	1.1	0.0	-0.8	2.8	1.2
Feb	-0.4	-1.1	2.4	1.8	0.4	0.7	0.0	1.2	1.0	1.6
Mar	-0.5	-71.0	-1.6	-1.6	-0.2	-0.3	0.2	0.5	-2.2	-1.0
Apr	-2.6	-1.7	-3.3	-2.0	-0.8	-0.5	-0.1	-0.2	-2.8	-1.3
May	1.7	0.8	-5.7	-2.3	-3.2	-1.0	3.0	1.1	-7.0	-2.2
Jun	-4.7	-3.6	-3.6	-1.0	-4.5	-1.7	-1.0	-0.6	-12.8	-2.2
Jul	-5.5	-2.1	-2.7	-0.6	-4.1	-2.0	2.3	0.8	-16.4	-1.2
Aug	-4.7	-1.4	4.3	2.3	-9.0	-2.9	2.4	1.0	1.6	0.8
Sep	-3.6	-1.3	10.6	1.9	1.5	0.7	2.2	0.8	4.6	1.3
Oct	-2.7	-1.2	5.7	1.6	5.8	2.3	-0.3	-0.1	8.9	0.7
Nov	0.2	0.0	10.5	0.9	9.1	1.0	0.8	1.3	11.4	1.7
Dec	-0.3	-1.3	7.4	1.6	3.4	2.7	0.1	0.5	6.1	1.9
summer	-5.0	-2.3	-0.7	0.3	-5.9	-2.2	1.2	0.4	-9.2	-0.9
Spring	-2.0	-0.8	8.9	1.5	5.5	1.3	0.9	0.7	8.3	1.3
winter	-0.6	-1.7	4.0	1.4	1.9	1.5	0.0	0.3	3.3	1.6
Autumn	-0.5	-24.0	-3.5	-2.0	-1.4	-0.6	1.0	0.5	-4.0	-1.5
Annual	-2.0	-7.2	2.2	0.3	0.0	0.0	0.8	0.5	-0.4	0.1

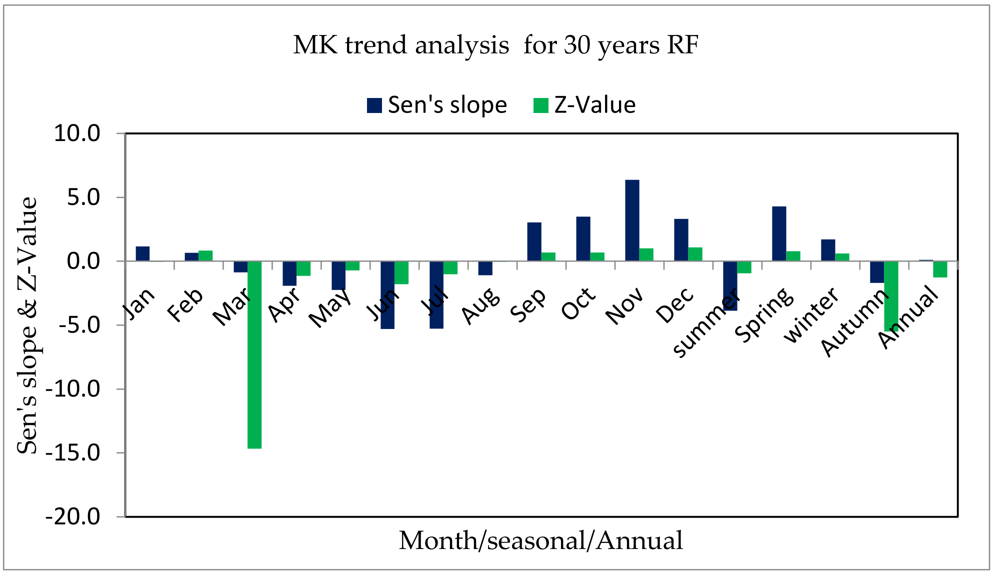

Figure 7. Means values of Stations for Sen's Slope Value, and Z-Value

Preprints (www.preprints.org) | NOT PEER-REVIEWED | Posted: 11 July 2022 doi:10.20944/preprints202207.0158.v1

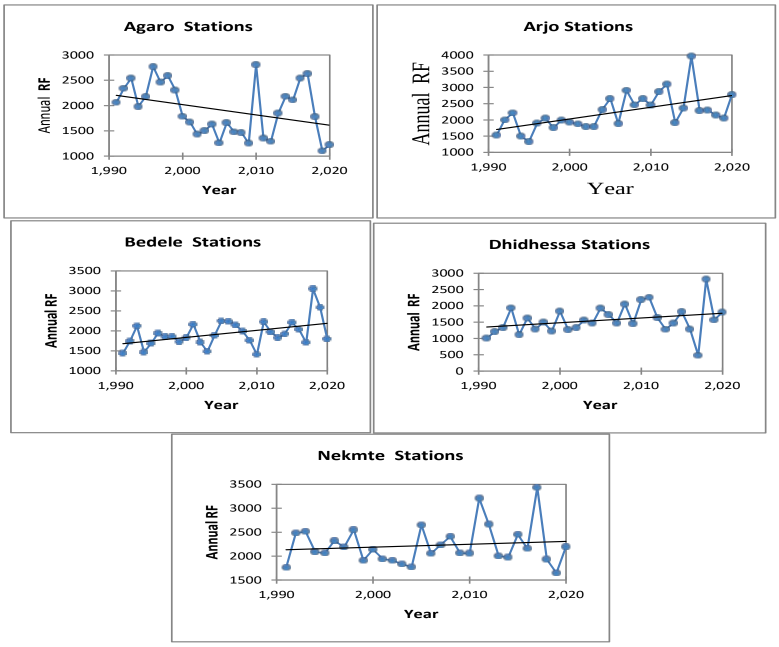

Figure 8. Trends of Observed Rainfall

3.1.2. Test Temperature Trend Analysis on the Study Area

Long-term trends in the observed and adjusted time series data were identified using the MK test, with linear evolution of the data represented by Kendall–Theil Robust Lines. This non-parametric MK test is very suitable for assessing the variability of hydrological systems. Trend analysis was used to examine whether there was an upward, downward, or no trend in the value points of the data. This paper also used ITAM to identify time series data trends in precipitation, temperature, and runoff. To assess the reliability of the ITAM, the test results were compared with MK and Sen's cross-sectional estimates.

Annual min and max temperatures in the Dhidhessa Sub-basin (1991 to 2020) increased by 0.06°c and 0.15°c, respectively. The annual temperature in this sub basin has risen at a rate of 0.11°c per decade. As shown in the exhibit (Figure 9), while the average maximum temperature is increasing by 0.11°c per decade, the average minimum temperature is decreasing by 0.07°c per decade in the sub basin. The means of all stations, as well as Sen's slope and z-value, are shown in (Table 4).

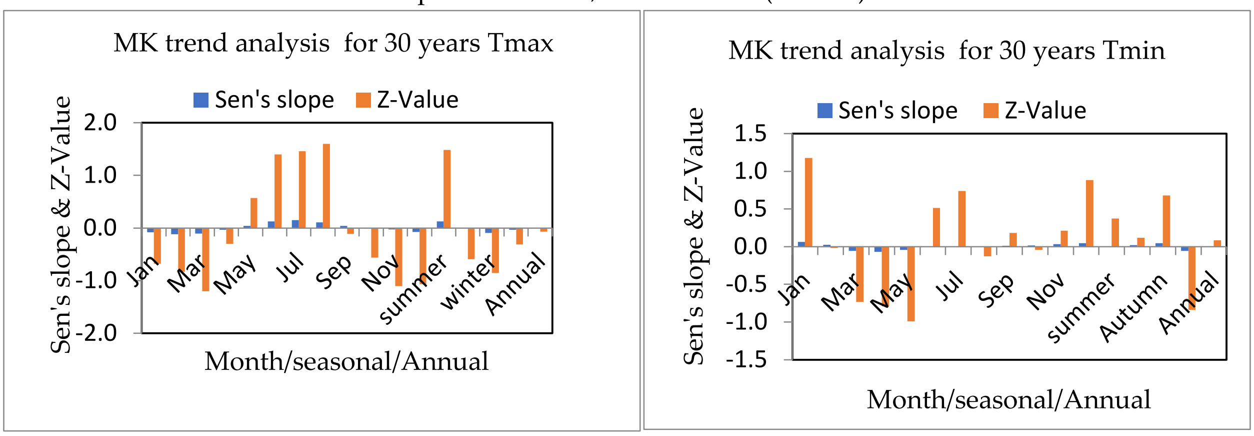

a b

Figure 9. a) Tmax b) Tmin, for means of Sen's Slope Value, and z-value

Table 4. a) Max b) Min Temp Sens Slope value and Mann-Kendall Trend Test

Preprints (www.preprints.org) | NOT PEER-REVIEWED | Posted: 11 July 2022 doi:10.20944/preprints202207.0158.v1

Tmax(1991-2020)										
Month	Agaro		Arjo		Bedele		Dhidhessa		Nekemte	
	Sen's slope	Z-Value	Sen's slope	Z-Value	Sen's slope	Z-Value	Sen's slope	Z-Value	Sen's slope	Z-Value
Jan	0.0	0.3	-0.2	-0.4	-0.2	-2.2	-0.1	-2.1	0.0	1.0
Feb	0.0	0.1	-0.3	-1.7	-0.1	-1.7	-0.1	-1.4	-0.1	0.6
Mar	0.0	-0.2	-0.3	-1.9	-0.2	-3.4	0.0	-0.7	-0.1	0.2
Apr	0.0	0.7	-0.2	-1.7	-0.1	-1.1	0.0	0.0	0.0	0.6
May	0.0	0.0	-0.1	-2.0	0.0	0.8	0.2	1.9	0.1	2.1
Jun	0.1	1.2	0.0	0.7	0.1	1.0	0.2	1.3	0.3	2.9
Jul	0.2	0.9	0.1	2.2	0.1	2.5	0.1	0.4	0.2	1.3
Aug	0.3	2.6	0.1	1.5	0.0	0.3	0.1	1.4	0.1	2.2
Sep	0.2	0.2	0.0	0.5	-0.1	-1.5	0.0	-0.8	0.0	1.1
Oct	0.1	0.5	0.0	0.3	-0.1	-2.1	-0.1	-1.3	0.0	-0.1
Nov	0.2	0.9	-0.1	-0.5	-0.1	-3.5	-0.1	-2.3	0.0	-0.1
Dec	0.0	0.5	-0.1	-1.3	-0.2	-1.1	-0.1	-2.4	-0.1	-1.1
summer	0.2	1.5	0.1	1.5	0.1	1.2	0.1	1.1	0.2	2.1
Spring	0.2	0.5	0.0	0.1	-0.1	-2.4	-0.1	-1.5	0.0	0.3
Autumn	0.0	0.3	-0.2	-1.1	-0.2	-1.7	-0.1	-2.0	-0.1	0.2
winter	0.0	0.2	-0.2	-1.9	-0.1	-1.2	0.0	0.4	0.0	1.0
Annual	0.1	0.6	-0.1	-0.4	-0.1	-1.0	0.0	-0.5	0.0	0.9

a

Tmin(1991-2020)										
Month	Agaro		Arjo		Bedele		Dhidhessa		Nekemte	
	Sen's slope	Z-Value	Sen's slope	Z-Value	Sen's slope	Z-Value	Sen's slope	Z-Value	Sen's slope	Z-Value
Jan	0.0	-0.1	0.1	1.8	0.0	0.6	0.2	1.8	0.0	1.8
Feb	0.0	-0.1	0.0	0.6	-0.1	-2.0	0.2	1.9	0.0	-0.5
Mar	0.0	0.3	-0.1	-0.9	-0.1	-2.0	0.0	0.5	-0.1	-1.5
Apr	0.0	-0.2	-0.1	-1.1	-0.1	-1.8	-0.1	-0.1	-0.1	-0.7
May	0.0	0.4	0.0	-1.9	-0.1	-2.0	-0.1	-0.5	-0.1	-1.0
Jun	0.0	0.0	0.0	1.2	0.0	0.0	-0.1	-0.8	0.1	2.2
Jul	0.0	0.5	0.1	2.7	0.0	-0.1	-0.1	-2.8	0.1	3.4
Aug	0.0	-0.1	0.0	1.4	0.0	-1.0	-0.1	-2.2	0.0	1.1
Sep	0.1	0.5	0.1	1.7	0.0	-2.2	-0.1	-1.9	0.0	2.9
Oct	0.1	0.1	0.1	0.5	0.0	-0.7	-0.1	-1.3	0.0	1.2
Nov	0.0	-0.3	0.1	0.7	0.0	0.4	0.0	-0.4	0.0	0.6
Dec	0.0	-0.1	0.1	0.7	0.1	1.9	0.1	0.8	0.0	1.1
summer	0.0	0.2	0.0	1.8	0.0	-0.4	-0.1	-1.9	0.1	2.3
Spring	0.0	0.1	0.1	1.0	0.0	-0.8	-0.1	-1.2	0.0	1.6

Preprints (www.preprints.org) | NOT PEER-REVIEWED | Posted: 11 July 2022 doi:10.20944/preprints202207.0158.v1

Autumn	0.0	-0.1	0.1	1.0	0.0	0.2	0.1	1.5	0.0	0.8
winter	0.0	0.2	-0.1	-1.3	-0.1	-2.0	-0.1	0.0	-0.1	-1.1
Annual	0.0	0.1	0.0	0.6	0.0	-0.7	0.0	-0.4	0.0	0.9

b

As a season, the maximum temperature in the study area increased by 0.1°c in summer, while the maximum temperature in winter increased by 0.1°c and the other two seasons by 0.0°c in each year of the time series between 1991 to 2020 decreased. Similarly the minimum temperature of Dhidhessa sub-basin showed an increasing trend with a minimum value of 0.01°c during summer, autumn and winter. The autumn season also decreased by 0.1°c, and the maximum temperature of the Dhidhessa sub-basin showed a decreasing trend with minimum values of 0.034°c, 0.004°c, and 0.09°c in autumn, winter, and spring, respectively , there is also summer season increased as shown in (Figure 10 a and b). In contrast to the other two seasons, the maximum temperature of the summer season showed the highest increase of 0.1°c per decade, while the minimum temperature of the autumn season showed a decrease of 0.1°c in value as (Table 4.a & b) in general, the variation of temperature is shown in decades rather than in years.

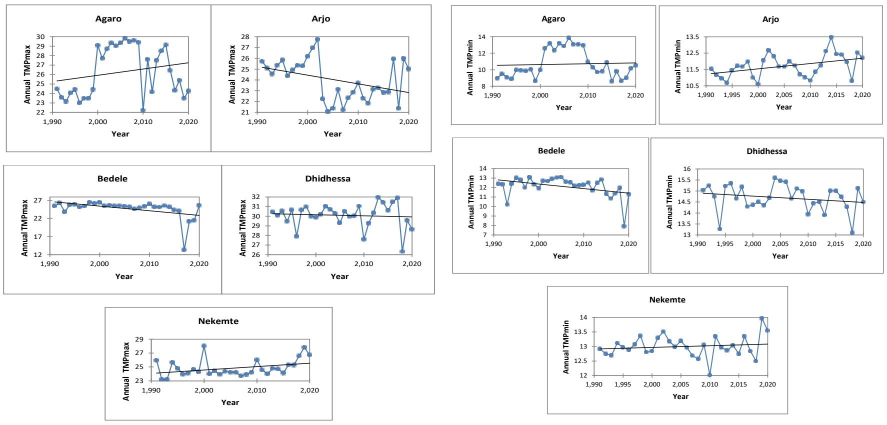

a b

Figure 10. a)Tmax and b) TminTrend Test Applied at Annual on Temperature

3.1.3. Stream flow Trends Test Analysis over the Study Area

Trend analyzes tests require the data to be sequentially independent. This is the main thing estimates for parametric and nonparametric tests. Most studies of trend analysis have assumed that the recorded hydroclimatological time series are usually independent series. Whereas, some variables such as annual mean data and low density may show statistically significant serial correlation. The MK trend test in the Dhidhessa sub-basin was on an annual time scale (i.e. p-value and Sen's slope value) and was to examine and identify trends that existed in the observed stream discharge data (Figure 11) with p-a smaller decrease is shown value is 0.724 and Sen's slope is 7.542. The average annual amount exceeded each year from 1991 to 2020 decreased in value by 0.031m³/s between each period and increased by 0.6m³/s over the decade, the seasonal flow rate (Figure 11).

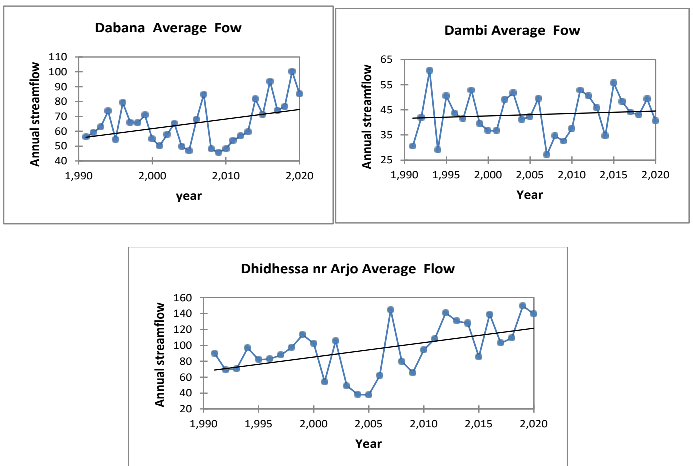

 doi:10.20944/preprints202207.0158.v1

Figure 11. Trend test Applied at Annual on Observed StreamFlow

3.2. Hydrological Modeling Result

3.2.1. Sensitivity Analysis

The sensitivity, calibration, and validation of the Dhidhessa SWAT hydrological model were carried out at a multi gauge site (Dambi, Dabana near Buno Bedele, Dhidhessa near Arjo, and Wama). These were created using available measured climate and stream flow data and a popular algorithm called SUFI-2 to reduce the uncertainty in future predictions. The outcomes of the sensitivity analysis of global sensitivity (GSA) was showed a few parameters which had direct relation and their impact on simulated stream flow resulted from the water yield remained after some losses passed through SWAT water balance systems showed at (Figure 12). The most sensitive parameters were screened and ranked based on the absolute values of the t-stat and the positivity and negativity of the p-values of the GSA descriptive ranking, as shown in (Figure 12). The GSA result showed eighteen (18) most sensitive parameters and was regarded as relevant to water balance components such as precipitation, evapotranspiration, surface runoff, groundwater, and lateral flow, which directly affected the total water yield in the sub basin, as shown in the table below (Table 5).

The most sensitive parameters were CN2.mgt, GW_DELAY.gw, and GWQMN.gw, ESCO.hru, GW_REVAP.gw, OV_N.hru, followed by SLSUBBSN.hru ranked after repeated model iteration numbers. The daily curve number condition II (CN2.mgt) was led the Dhidhessa SWAT model calibration system from the start to the end especially in controlling the direct surface runoff and total water yield (simulated stream flow). The overland flow parameter was Manning's coefficient parameters (OV_N.hru) also showed a direct impact on simulated stream flow that started after saturated soil storage. The rainfall adjustment factor (RFINC (...).sub) parameters were applied at the sub-basins level to correct underestimated mean annual rainfall amount during the first simulation.

The increased and decreased value of this parameter showed a direct relationship to simulated stream flow by increasing monthly rainfall amount. Manning's coefficients (CH_N2.rte), which are used to limit the flow out rate (discharge) at the main channel outlet, appear to be the most sensitive parameters in main channel routing. The surface lag time coefficient (SURLAG.bsn) is a surface runoff parameter that controls surface runoff by calculating concentration time from time travel and overland flow time. The deep recharging parameter (RCHRG_DP.gw) was used to control the ground water flow that returned as a return flow to the main channel stream flow. Because the deep aquifer recharge water increased as the value of this parameter increased, this was accounted for as a loss in the SWAT model throughout the calibration process. A detailed description of those relationships and their effects on calibrated monthly river discharge (discharge rate) and GSA sensitive parameter graphs can be found in the (Table 5 and Figure 12).

Table 5. Sensitive Parameters

Parameter Name	Fitted Value	Min_ value	Max_ value	t-Stat	P-Value
1:A__CN2.mgt	0.1	0.1	0.2	0.2	0.9
2:V__ALPHA_BF.gw	0.5	0.4	0.5	-1.2	0.2
3:V__GW_DELAY.gw	471.3	340.6	488.6	13.8	0
4:V__GWQMN.gw	-33.2	-39	10.7	-0.9	0.4
5:V__ESCO.hru	0.9	0.8	1	2	0.1
6:V__GW_REVAP.gw	0.1	0.1	0.1	-0.2	0.8
7:V__OV_N.hru	0.3	0.3	0.4	-1.2	0.2
8:V__SFTMP.bsn	-2.6	-3.9	-2.6	-0.5	0.6
9:A__SLSUBBSN.hru	-20.8	-31	-18	-0.3	0.8
10:A__SOL_AWC (...).sol	0	0	0	-1.4	0.2
11:A__SOL_K(..).sol	0	0	0	0.1	1
12:V__SURLAG.bsn	-3	-4.5	-1.9	0.9	0.4
13:V__RCHRG_DP.gw	1	1	1.3	-0.2	0.8
14:R__LAT_TTIME.hru	0.3	-0.2	0.6	1.1	0.3
15:R__CH_N2.rte	0	0	0.1	0.1	0.9
16:R__CANMX.hru	0.7	0.5	0.8	0.6	0.6
17:R__RFINC (...).sub	-0.6	-0.6	-0.3	0	1
18:R__CNCOEF.bsn	1.2	1.2	1.3	-0.6	0.6

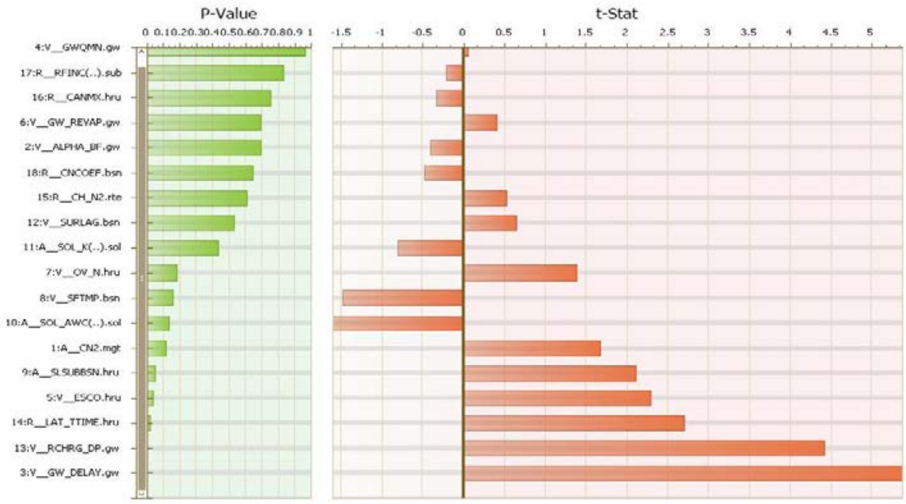

Figure 12. GSA Sensitive Parameters

3.3. Hydrological Model Calibration and Validation (SWAT)

3.3.1. Calibration model

Once the sensitivity parameters for the model have been identified, the next step is to calibrate and validate the model. Both manual and automated measurement procedures (using the SUFI-2) were used in this study. Initially, the curve number for moisture condition II (CN2.mgt), aquifer delay time (GW_DELAY.gw), existing soil water potential (SOL_AWC (...).sol), and soil evapotranspiration compensation coefficient (ESCO .hru) are the calibration values have been manually adjusted. For model calibration, Dhidhessa River data for 18 years (1994 to 2011) and validation (2012 to 2020) at each calibration station. Three years of data (1991-1993) were used for model warming. The performance of the model was evaluated for manual and automated calibration using R^2, N_{ES}, and P_{BIAS} statistical measures. The evaluation was performed on a monthly time scale, and the effect of statistical parameters obtained during measurement was 0.88 for R^2, 0.76 for N_{ES}, and 2.41% for P_{BIAS}. Flow density values indicate good agreement between observed and simulated. Figure (13) below shows the hydrograph for comparison during model calibration.

Preprints (www.preprints.org) | NOT PEER-REVIEWED | Posted: 11 July 2022 doi:10.20944/preprints202207.0158.v1

3.3.2. Validation model

Validation of model results is essential to enhance user confidence in model predictive capabilities. Nine (9) years of monthly baseline data (2012-2020) were used for model validation without any adjustment of the fitted value during the calibration period, and values of 0.80 for R^2, 0.77 for E_{NS}, and 9.2% for P_{Bias} were obtained (Figure 13).

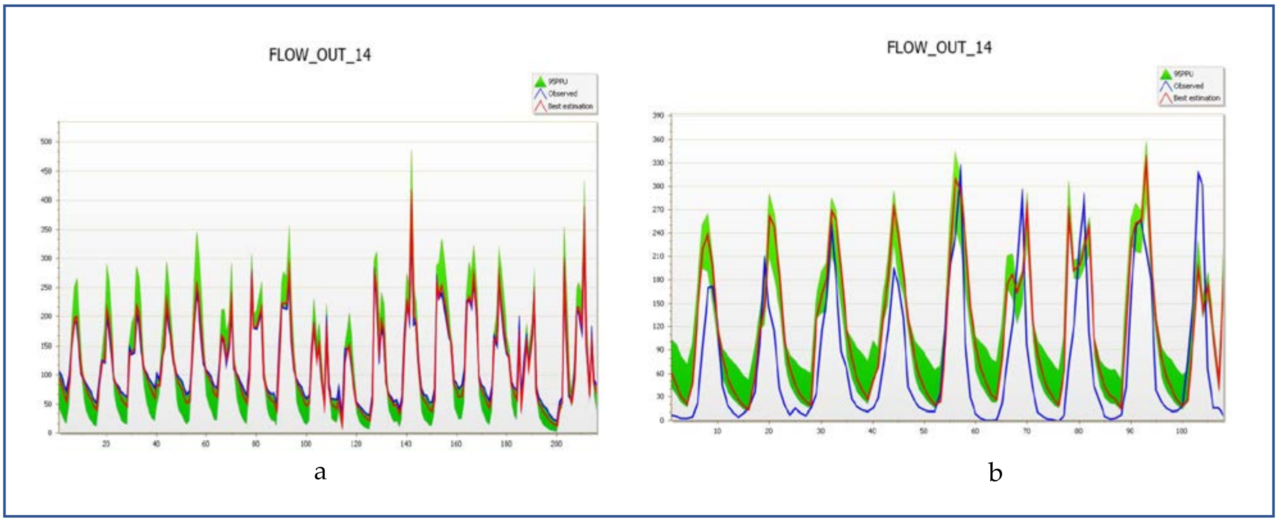

Figure 13. a). Stream flow Calibration for Dabana Station and b). Stream flow Validation for Dabana Station

3.4. Evaluation of Surface Water Availability in the Present Climate

3.4.1. Monthly, Yearly, and Yearly Climate

Figures 14 shows the seasonal minimum, maximum, and mean Dhidhessa Sub-basin temperatures, mean annual temperatures, and climatic seasons (spring, summer, winter, and autumn). During this reference period (1991-2020), the mean monthly temperature of the sub basin ranged from 11.25°c to 28.84°c, with a maximum and minimum monthly temperature of 20.98°c was found between 33.37°c and 8.26 °c to 15.86°c , respectively (Figure 14). Dhidhessa Sub-basin means annual minimum and maximum temperatures of 12.44°c and 26.01°c. Mean seasonal temperatures ranged from 12.74 to 24.25°c, 11.89 to 24.6°c, 11.82 to 27.01°c, and 13.32 to 28.19°c, summer, autumn, winter, and autumn) between the minimum and maximum temperatures.

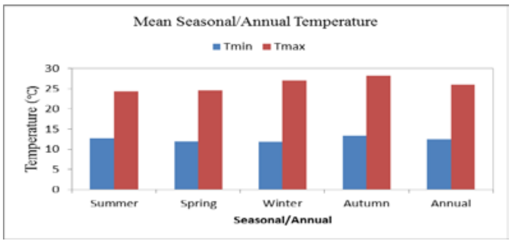

Figure 14. Relationship between mean seasonal Max and MinTemperatures

3.4.2. Water Balance Components of the Baseline Period (1991-2020)

In the most of time much water was lost as evaporation transmission and total losses, with 47.2mm and 3mm, respectively, of the mean annual rainfall captured over the Dhidhessa sub-basin in the baseline period of 160.9mm. The water yield retained as Dhidhessa current available water was 111.7mm, as shown in (Figure 15) below. The entire mean annual surface runoff as surface water availability was 57.3mm of this total water production. The total amount of water that percolates down to the shallow and deep aquifers each year was 49.6mm, with 6.7mm of lateral flow and 45.2mm of groundwater

 doi:10.20944/preprints202207.0158.v1

flow returning to the stream flow channel (Figure 15). The water that was permanently lost from the Dhidhessa sub-basins was deep aquifer recharging and transmission losses, whereas the other water balance components were used in the hydrological cycle of the sub-basins. The mean annual potential evapotranspiration was estimated to be 95.5mm in the sub-basin.

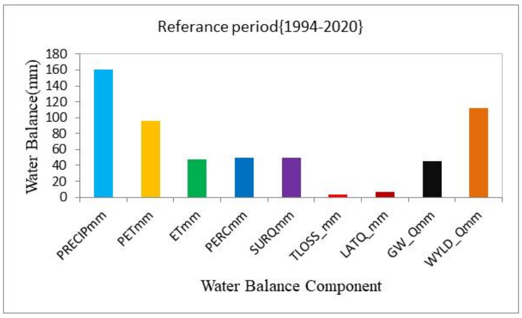

Figure 15. Dhidhessa Sub-basins Average Annual Water Balance Components

3.4.3. Monthly, Seasonal, and Annual Stream flow under Current Climate

Figure 16 shows the monthly, seasonal, and annual mean stream flow for the reference period (1991–2020). The rainy season months are August, September, and October, with peak flow rates of 324.6m³/s, 347.8m³/s, and 306.4m³/s, respectively (Figure 16a). The summer and spring seasons in this study area are long rainy wet seasons, with maximum mean seasonal stream flow rates of 254.9m³/s and 295.3m³/s, respectively. The autumn season, which is a short rainy season with 81.7m³/s, compared to a medium annual record and a low record in the winter (long dry) seasonal see (Figure 16b). The mean annual stream flow increased linearly from 1991 to 2020, with the highest flood occurring in 2019 with 100.1m³/s and the lowest stream flow occurring in 2009 with 45.6m³/s (Figure 16c).

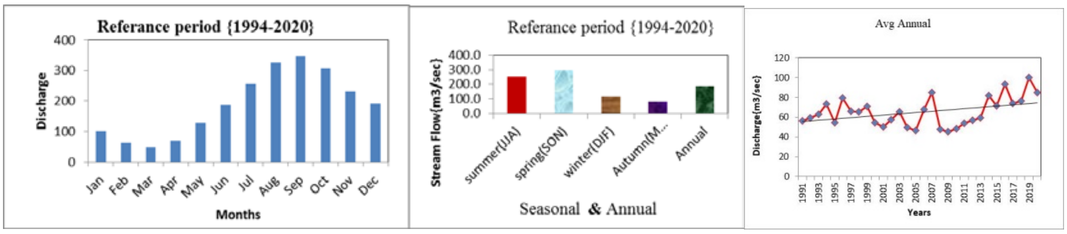

a b a

Figure 16. (a) Monthly, (b) Seasonally, and (c) Annual Mean Stream flow

3.5. Scenarios for Future Climate Change Signals

The change and trends detected monthly, seasonally, and annually of mean maximum and mean minimum temperature for each Representative Concentration Pathways (RCP) were summarized from a three-climate model (i.e. DMI-HIRHAM5, KNMI- RACMO22T, and SMHI-RCA4). The change in monthly mean temperature increased from 1.14°c to 1.89°c, 1.1°c to 2.2°c, 1.3°c to 2.1°c, 1.4°c to 2.3°c, 1.4°c to 2.1°c and 1.4°c to 2.1°c respectively DMI-HIRHAM5-RCP4.5, DMI-HIRHAM5-RCP8.5, KNMI-RACMO22T-RCP4.5, KNMI-RACMO22T-RCP8.5, SMHI-RCA4-RCP4.5 and SMHI-RCA4-RCP8.5 in short-term period (2044). In long-term period (2084) was 1.3°c to 1.9°c, 1.4°c to 1.5°c, 1.2°c to 1.9°c, 1.9°c to 2.1°c, 1.2°c to 2°c and 1.8°c to 2.3°c for RCP4.5 and RCP8.5 respectively DMI-HIRHAM5-RCP4.5, DMI-HIRHAM5-RCP8.5, KNMI-RACMO22T-RCP4.5, KNMI-RACMO22T-RCP8.5, SMHI-RCA4-RCP4.5 and SMHI-RCA4-RCP8.5 (Figure 17a).

Although all months showed a considerable rise over their baseline period, there was a discrepancy across months and climate scenarios for both time frames. For example, the emission scenario (RCP8.5) showed a significant change, while RCP4.5 showed a low-significant increase over the long-term period of 2084 from the baseline period, and even in the long-term period of 2084 from January to March and July to September, RCP4.5 showed a significant increase over the months under the RCP4.5 and RCP8.5 scenarios (Figure 17b).

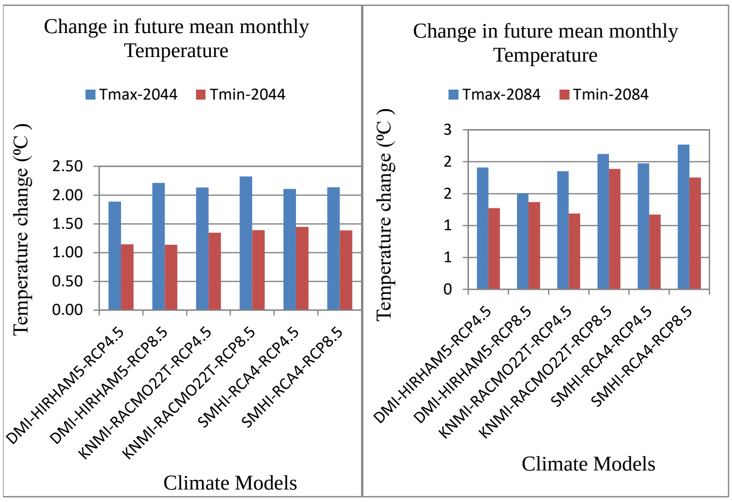

a b

Figure 17. a) 2044 and b) 2084, Change in Future Mean Monthly Temp by two faces

Future mean monthly temperature changes for a) RCP4.5-2044, and RCP8.5-2044, b) RCP4.5-2084, and RCP8.5-2084 are shown in (Figure 18). The monthly change in mean maximum temperature increased from 2.7°c to 2.9°c, 2.5°c to 2.8°c, 3.1°c to 3°c, 3.1°c to 3.2°c, 3.2°c to 2.6°c and 3°c t o 2.9°c respectively DMI-HIRHAM5-RCP4.5, DMI-HIRHAM5-RCP8.5, KNMI-RACMO22T-RCP4.5, KNMI-RACMO22T-RCP8.5, SMHI-RCA4-RCP4.5, and SMHI-RCA4-RCP8.5 in short-term period (2044). In long-term period (2084) was 2.5°c to 3.13°c, 2.4°c to 2.6°c, 2.5°c to 2.7°c, 2.8°c to 3°c, 2.8°c to 3°c and 3.1°c to 3.4°c for RCP4.5 and RCP8.5 respectively. The change in monthly mean minimum temperature increased from 1.44°c to 1.45°c, 1.2°c to 1.7°c, 1.4°c to 1.6°c, 1.1°c to 1.4°c, 1°c to 1.6°c and 1.3°c to 1. 8°c respectively DMI-HIRHAM5-RCP4.5, DMI-HIRHAM5-RCP8.5, KNMI-RACMO22T-RCP4.5, KNMI-RACMO22T-RCP8.5, SMHI-RCA4-RCP4.5, and SMHI-RCA4-RCP8.5 in short-term period (2044). In long-term period (2084) was 1.2°c to 1.9°c, 1.5°c to 2.1°c, 1.4°c to 1.6°c, 1.7°c to 2.4°c, 1.2°c to 2°c and 1.2°c to 2.4°c for RCP4.5 and RCP8.5 respectively DMI-HIRHAM5-RCP4.5, DMI-HIRHAM5-RCP8.5, KNMI-RACMO22T-RCP4.5, KNMI-RACMO22T-RCP8.5, SMHI-RCA4-RCP4.5, and SMHI-RCA4-RCP8.5 showed at (Figure 18a).

The change of mean temperature over the Dhidhessa in spring season, winter season and annual for the short-term period (2044) (Figure 18), increased by 0.8°c, 1.6°c, and 0.3°c, and summer, and autumn season was decreased by 0.9°c, and 0.1°c under intermediate emission RCP4.5 scenarios respectively. Similarly, the short-term period of 2044 means temperature in spring season, winter season, and annual increased by 0.9°c, 1.6°c, and 0.3°c, and summer, and autumn season was decreased by 1.0°c, and 0.2°c under high emission RCP8.5 scenarios respectively compared with the baseline period(Figure 18). Under the long-term period (2084), the signal change of mean temperature in spring season, winter season, autumn season, and annual for the long-term period (2084) increased by 0.8°c, 0.5°c, 0.0°c, and 0.2°c, and the other in summer was decreased by 0.6°c, under intermediate emission RCP4.5 scenarios respectively. Similarly, the long-term period of

 doi:10.20944/preprints202207.0158.v1

2084 means temperature in spring season, winter season, autumn season, and annual increased by 1.0°c, 0.0°c, 0.7°c, and 0.3°c, and the other in summer was decreased by 0.4°c, under high emission RCP8.5 (Figure 18) scenarios respectively compared with the baseline period.

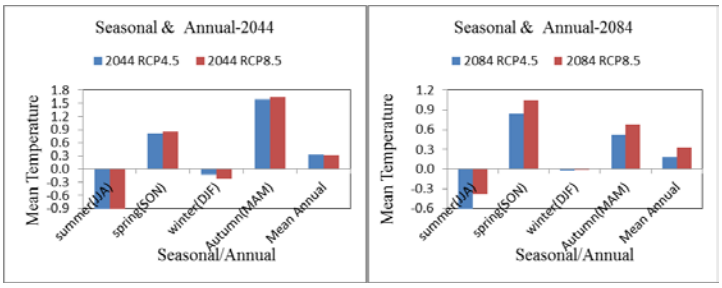

a b

Figure 18. a) 2044 and b) 2084; Change in Mean seasonal and annual future Temperature

3.6. Impact of Climate Change on Future Surface Water Availability

3.6.1. Future Components of the Water Balance

There is a mixed percent change for each water balance component from projected future climate scenarios at mean annual (i.e. 2044 (2030-2059) and 2084 (2070-2099) time steps over the Dhidhessa Sub-basins modeled from a three-climate model under each RCP at a monthly time step. Under the short-term period (2044), the percent change in mean annual water balance components such as potential evapotranspiration and evapotranspiration increased insignificantly by 15.9%, and 6.5%, respectively, while precipitation, percolation of water, surface runoff, transmission losses, lateral flow, groundwater flow, and water yield dramatically decreased by 5.6%, 42.6%, 44%, and 2.1%, respectively. However, a significant decrease in percent change in return flow and lateral flow is due to a decrease in percent change in water percolation at the vadose root system. This percolation of water returned the total water yield from Dhidhessa to the main channel stream flow through the lateral and returns (groundwater) flow.

This decreased percent change in total water production over the study region is a major issue for agricultural development and groundwater resource development in this sub basin (Figure 19). Except for potential evapotranspiration and evapotranspiration, which increased by insignificant values with 22.4 percent and 11.6 percent change from the baseline period, all water balance components showed an insignificant decrease in future percent change in the long-term period (2084), which is the same as the short-term period (2044). The percent change in mean annual water balance components such as precipitation, percolation of water, surface runoff, transmission losses, lateral flow, groundwater flow, and water yield was significantly reduced during this period, with 1.6%, 42.7%, 43.1%, 3.4%, 29.1%, 47.3%, and 5.7%, respectively, compared to the baseline period.

The significantly reduced percent change in total water output will put agricultural development at risk, and domestic water supply will be scarce during this time, which will have a direct impact on livelihoods in the Dhidhessa Sub-basins. As shown in (Figure 19), respectively), the potential evapotranspiration rose as a result of significantly higher trends in the mean annual temperature (2070–2099).

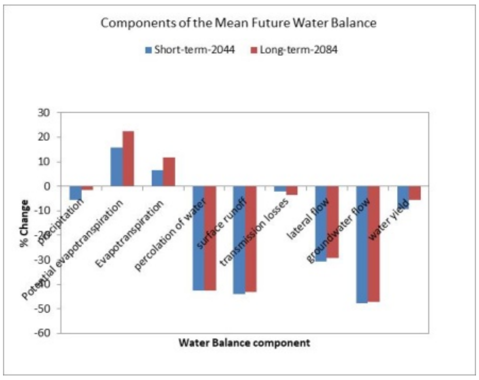

Figure 19. water balance components percent

Except for potential evapotranspiration and evapotranspiration, all water balance components indicated a decreased percent change in the short-term period of 2044 under the emission scenario (RCP4.5). In the long-term period of 2084, there was a negative influence on the Dhidhessa Sub-basins, with all percent changes of future water balance components decreasing from baseline, except potential evapotranspiration and evapotranspiration, both strongly decreasing with percent change. Under this scenario, the decreased percent change in all components over the long run (2084) was the consequence of just an increased percent change in potential evapotranspiration and evapotranspiration. Precipitation reduced by 5.6% and 1.6% in both periods (i.e., 2044 and 2084) respectively, percent change from the reference period (1991–2020) in this scenario (Figure 20). Potential evapotranspiration increased by 15.9% and evapotranspiration was also increase by 22.4% from the baseline period under the high emission scenario (RCP8.5) (Figure 20) under short and long-term period respectively.

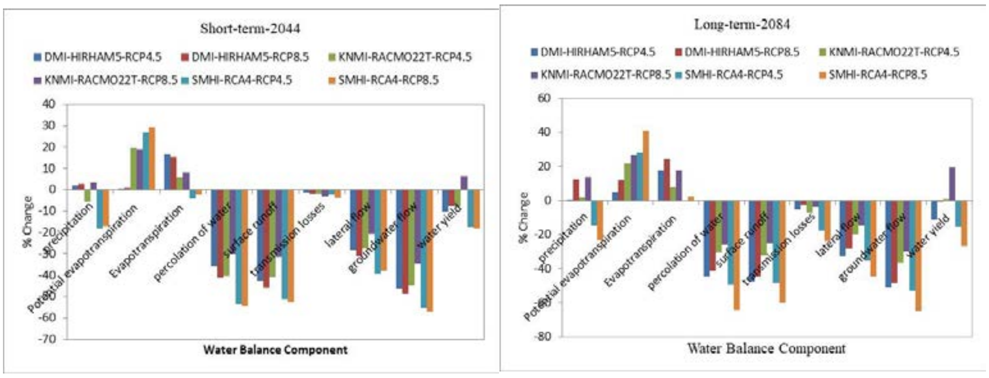

a b

Figure 20. Percent change in mean annual water balance components under two rcp scenarios: a) 2044 and b) 2084.

3.6.2. Future Monthly Mean Flow

The month-flow rate modeled over (Dhidhessa Sub-basins) for two time periods (i.e., 2030-2059 and 2070-2099) revealed a mixed percent change from the reference p riod (1991-2020). Under the short-term period (2044) for models DMI-HIRHAM5-RCP4.5, DMI-HIRHAM5-RCP8.5, KNMI-RACMO22T-RCP4.5, KNMI-RACMO22T-RCP8.5, SMHI-RCA4-RCP4.5, and SMHI-RCA4-RCP8.5 the mean stream flow percent change in the main channel river is decreased with 10.1%, 6.9%, 8.9%, 19% and 20.7% from a baseline line period respectively, but KNMI-RACMO22T-RCP8.5 model is increased by 5.7% insignificant. The decreased percent change in future stream flow in Dhidhessa Sub-basins is critical in case of survival of rain-fed agricultural production with supplementary irrigation system (spate and pump irrigation water).

Under the long-term period (2084), the mean stream flow over Dhidhessa Sub-basins exhibits a significant increase percent change for DMI-HIRHAM5-RCP8.5, KNMI-

Preprints (www.preprints.org) | NOT PEER-REVIEWED | Posted: 11 July 2022 doi:10.20944/preprints202207.0158.v1

RACMO22T-RCP4.5, and KNMI-RACMO22T-RCP8.5 from their baseline period in opposite to short-term period (Figure 21b). The 12.9%, 15.6%, and 28.6% decreases in % change over Dhidhessa Sub-basins in DMI-HIRHAM5-RCP 4.5, SMHI-RCA4-RCP4.5, and SMHI-RCA4-RCP8.5, respectively, resulting in a significant decrease in percent change from the baseline period (Figure 21a). Because the contribution of the Dhidhessa Sub-basins river comes from the steep slope area of the topography of the Dhidhessa watershed and other areas located around such a region, this significant decrease in future stream flow presents a difficult scenario in the socio-economics of the study area subsequently.

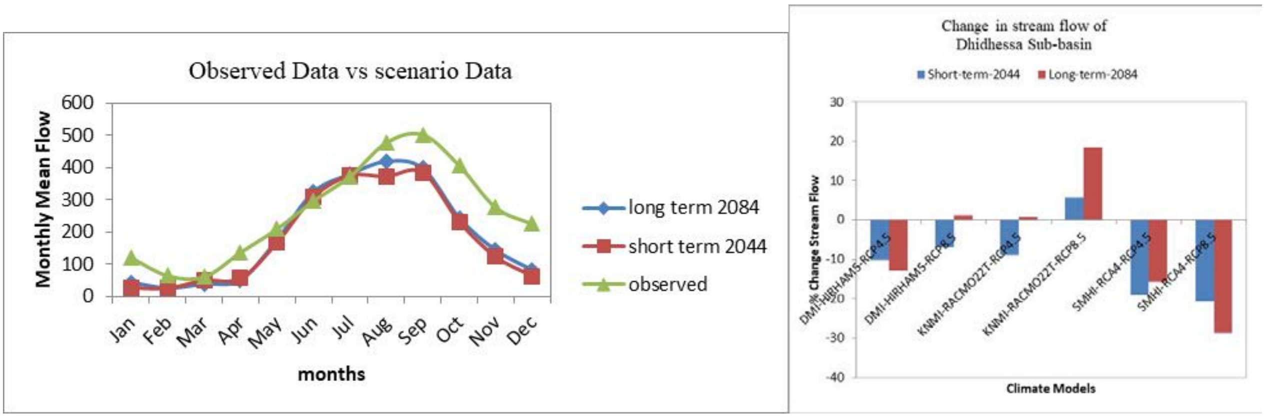

Figure 21. Change in stream flow in the dhidhessa basin under scenarios from 2044(2030-2059) and 2084(2070-2099).

With RCP4.5, the mean monthly stream flow for the short-term period (2044) will increase insignificantly in March, with May to September showing the only considerable increase (72.1%) from the baseline period. The percentage change in these three situations will be minimal in January, February, March, April, October, November, and December, respectively. In March and May to September, the sub-basins will see a mild increase in the mean monthly percent change in stream flow, with a change interval of 2.3% to 124.5% change from their baseline period. The exceptional instance will be seen in the long-term period (2084) of RCP4.5, which will show an inclination for months from May to September, with incremental percent change intervals ranging from 12.8% to 60.3%.

In general, the RCP4.5 long-term period will see a decreased change from January to April and October to December, with decrement intervals ranging from 12.6% to 89.2% and 22.9% to 74.3%, respectively, from the baseline period (1991-2020).For both periods (i.e. 2044 and 2084), the mean monthly future stream flow percent change under RCP8.5 shows a mixed change from the baseline period, similar to RCP8.5 scenarios. In the short-term period (2044) of this scenario, the mean monthly stream flow of SMHI-RCA4-RCP4.5 percent change will prefer to swing between interval changes of -91.5% and 86.5%. February had the highest percentage loss with -91.5%, while July had the highest and most dominant shift with a large gain value (+86.5%) over the reference period (Figure 22).

Overall, this long-term period of RCP8.5 will see a decline in change for KNMI-RACMO22T-RCP8.5, with changes ranging from -67.3 percent to 243.8 percent lower than the baseline period (1991-2020). During this time, the Dhidhessa Sub-basins main channel stream flow percent change will be at its lowest in February, at 67.3 percent, and at its highest in June, at 243.8 percent. The sub basin stream flow will see a minor reduction for the rest of this DMI-HIRHAM5-RCP8.5 scenario's months in 2084, with a decrement interval of 46.5 percent to 59.5 percent (Figure 22b).

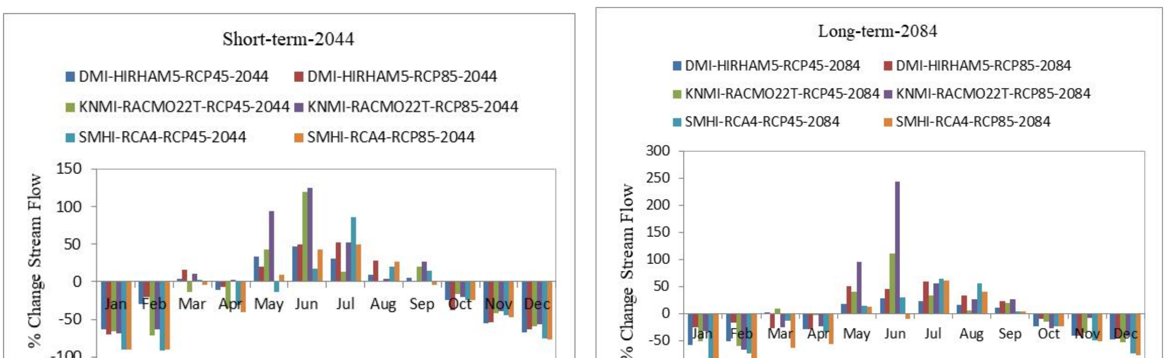

Preprints (www.preprints.org) | NOT PEER-REVIEWED | Posted: 11 July 2022 doi:10.20944/preprints202207.0158.v1

a b

Figure 22. a) 2044 and b) 2084; Percentage Change in Mean

3.7. Monthly Flow for RCP Scenario

3.7.1. Average Seasonal and Yearly Flows in the Future Climate

The Dhidhessa Sub-basins stream flow will undergo the maximum incremental percent change in both annual and seasonal periods (i.e. summer, spring, winter, and autumn). Stream flow significantly decreased in spring, winter, autumn, and annual with 20.2%, 67.4%, 67.4%, and 10% respectively, while summer season increased by 43.1%, respectively in short-term, from the baseline period (Figure 23). This lower percent change in stream flow over this study area poses a risk to the sub-basins water sector development (Figure 23). The stream flow in the main channel river over the Dhidhessa Sub-basin is expected to fail under the scarcity of water resource availability over the long-term period (2084). As shown (Figure 23) decreased in the following for both annual and three-season periods, except summer seasons, with 14.7%, 58.1%, 3.3%, and 6.3% change in spring, winter, autumn, and annual, respectively. And summer, with 51.1% from baseline increased. The reduction in mean yearly water supply resulted in a considerable decrease in average yearly flow throughout this period.

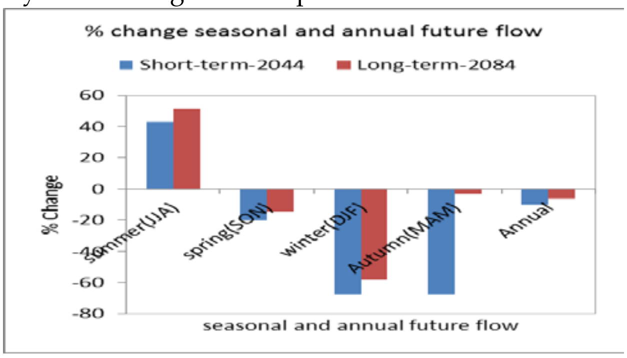

Figure 23. Change in seasonal and annual future flow percentages from the baseline period

3.7.2. Analysis of Uncertainties

Uncertainties in projected changes in the hydrological system arise from the following: internal variability of the climate system,

1) uncertainty in future greenhouse gas,
2) the translation of these emissions into climate change by GCMs/RCMs,
3) hydrological model uncertainty,
4) uncertainty from insufficient field data at all scales ([36]), and
5) uncertainty of downscaling techniques [37].

In general, the sources of uncertainties of climate scenarios are multiple. The climate system itself is too complex to be represented in a numerical model and contains a number of assumptions and parameterizations that each climate modeling centers approach differently. Uncertainties in climate scenarios and RCM/RCP outputs may be large [38]. The uncertainties related to SWAT model in this work could be as follows: (1) the relationship

Preprints (www.preprints.org) | NOT PEER-REVIEWED | Posted: 11 July 2022 doi:10.20944/preprints202207.0158.v1

between the predictor and predict and is achieved by only considering the data statistical condition, i.e., the model does not take into consideration the physical nature of the catchments (major drawback), (2) it requires high-quality data for model calibration; and (3) the model is highly sensitive to the choice of predictor variables and empirical transfer scheme. Parameter uncertainties and structural deficiencies in the hydrological models that are used for impact assessments are others sources of uncertainties. This is why different hydrological models may give different stream flow results for a given input [38].

The study area uncertainties are except for increases in the short-term scenarios (2044) and a slight shift in the rainfall coefficient variation of the long-term future scenario (2084), the coefficient variation of the yearly distribution of rainfall and evapotranspiration in the sub-basins for the future scenario is largely identical to that of the baseline scenario (Figure 24). In general, the summer annual rainfall amount is lower in the long-term (2084) than in the baseline period, with less considerable uncertainty. The uncertainty of future mean annual surface runoff depth was high, with a rise in short-term coefficient variation (2044) balanced by a decrease in the long-term scenario (2084) from the baseline period.

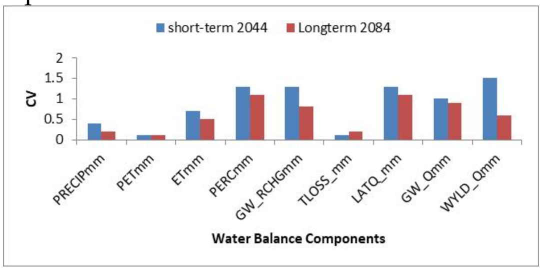

Figure 24. Coefficient variation in water balance components

Figure 25 shows whether or not hydrologic uncertainty is considerable for future generated runoff in the Dhidhessa Sub-basins. The discharge generated for the short term (2030–2059) was positioned between the two boundaries from January to June and September to November, indicating that the influence of climate change was minimal during this time (the change in discharge was because of other propagated uncertainty). However, hydrologic uncertainty was not expected for discharge created for the long-term scenario (2070–2099) from September to December because the discharge was generated outside of boundaries, indicating that the change in discharge was due to climate change. Therefore, the climate was relevant. In general, the generated discharge was placed outside of the two bounds; climate change influence is more significant in this Sub-basin than the other propagated uncertainty on the amount of future runoff.

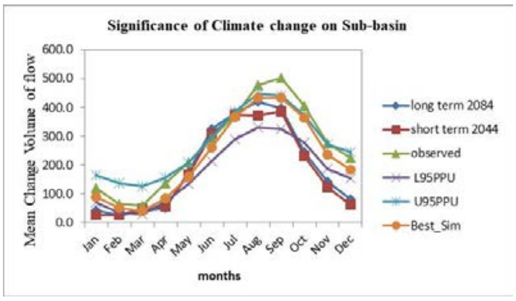

Figure 25. Uncertainty in baseline and future flow rate

4. Conclusion

This study is an effort to evaluate the impact of climate change on the availability of surface water resources in the Dhidhessa Sub basin in the lower Abbay basin. The climate model framework baseline to the period 1991–2020 and is used to forecast future impacts in two periods for the short period 2030 to 2059 and the long period 2070 to 2099. The short period (2030–2059) and long-term (2070–2099) assuming three-year warming. Prior

 doi:10.20944/preprints202207.0158.v1

to using the SWAT model directly, bias correction was conducted on the future precipitation and temperature datasets for the RCP4.5 scenario, producing a bias-corrected RCM output of 4.5 watts per square meter (W/m2), and projected for the RCP8.5 scenario RCM bias-corrected at 8.5 watts per square meter (W/m^2). The findings of the annual and quadrennial MK trend tests, as well as Sen's cross-sectional analysis, indicated a mixed trend. The average rainfall amount over the Dhidhessa Sub-basin decreased insignificantly between 1991 and 2020.

The average annual precipitation in the spring season (SON) declined dramatically, but it grew insignificantly in the summer (JJA), winter (DJF), and autumn (MAM). The minimum temperature of Dhidhessa sub-basin showed a non-negligible value of 0.1°c, for summer, autumn and winter seasons respectively, and a decrease of 0.1°c in autumn season, the maximum temperature of Dhidhessa sub-basin showed a decreasing trends minimum values of 0.034°c, 0.004°c, and 0.09°c during autumn, winter, and autumn respectively, and an increase of 0.1°c in summer season. The stream flow in the Dhidhessa Sub-basins was observed to be insignificantly lowered during of the spring, but significantly higher in summer, winter and autumn during the decade. Sensitivity analysis of hydrological model of Dhidhessa Sub-basins SWAT was performed with global sensitivity analysis (GSA). CN_2.mgt, GW_DELAY.gw, and GWQMN.gw, ESCO.hru, GW_REVAP.gw, OV_N.hru, followed by SLSUBBSN.hru, were the most sensitive parameters, which showed the direct influences stream flow. CN_2.mgt showed a direct relationship by increasing simulated output stream flow as their value increased.

The performance of Dhidhessa Sub-basins SWAT model calibrated and validated at the main outlet Dhidhessa showed very good performance with $R^2 > 0.75$, $N_{ES} > 0.75$. This study also reproduced the performance of the SWAT Drift model which performed very well with stream flow $R^2 > 0.75$ and N_{ES} value > 0.75. Overall, the model performance can be considered very good based on Percent of biased (P_{BIAS}) capturing observed stream flow rates and hydrographic patterns. The change of mean temperature over the Dhidhessa in spring season, winter season and annual for the short-term period (2044), increased by 0.8°c, 1.6°c, and 0.3°c, and summer, and autumn season was decreased by 0.9°c, and 0.1°c under intermediate emission RCP4.5 scenarios respectively. Similarly, the short-term period of 2044 mean temperature in spring season, winter season, and annual increased by 0.9°c, 1.6°c, and 0.3°c, and summer, and autumn season was decreased by 1.0°c, and 0.2°c under high emission RCP8.5 scenarios respectively compared with the baseline period.

Under the long-term period (2084), the signal change of mean temperature in spring season, winter season, autumn season, and annual increased by 0.8°c, 0.5°c, 0.0°c, and 0.2°c, and the other in summer was decreased by 0.6°c, under intermediate emission RCP4.5 scenarios respectively. Similarly, the short-term period of 2084 means temperature in spring season, winter season, autumn season, and annual increased by 1.0°c, 0.0°c, 0.7°c, and 0.3°c, and the other in summer was decreased by 0.4°c, under high emission RCP8.5. The mean annual precipitations evaluated over Dhidhessa Sub-basins will likely reduced by 5.6% and 1.6% in both periods (i.e., 2044 and 2084) and under scenario RCP4.5 and RCP8.5, 1.66%, 1.71% respectively declined for the short-term period of 2044. Even if there is a difference between each scenario, concerning the direction projected precipitation change, the long-term period of 2084 showed a declined trend with 2.5% RCP 8.5while RCP 4.5 will experience the increased percent change of 4.7%.

The totals mean annual water yield likely decreases by 11.1% and 5.2% for all models respectively under RCP4.5and RCP8.5 scenarios. The mean annual total water yield predicted over Dhidhessa Sub-basins will experience a decrease by percent change with 9.2% for the short period of 2044 and a decline of 5.7% for 2084. The stream flow under Annual and four seasons likely in 2044 Stream flow significantly decreased in spring, winter, autumn, and annual with 20.2%, 67.4%, 67.4%, and 10% respectively, while summer season increased by 43.1%, respectively in short-term, from the baseline period and under long-term (2084) period will experience a decrease except summer seasons, with 14.7%, 58.1%, 3.3%, and 6.3% change in spring, winter, autumn, and annual, respectively, and summer, with 51.1% from baseline peaked. On average, the stream flow projected in summer seasons will likely to a positive impact over Dhidhessa Sub-basins change by 43.1%, in short-term and 51.1% in long-term, respectively while the other season will experience to decrease in two faces.

Author Contributions: Conceptualization, Damtew.D.; methodology, Damtew.; software, Damtew.D.; Validation, Damtew.D., A.D. and M.S.R.; system analysis, Damtew.D.; research, Damtew.D.; data processing, Damtew.D.; preparation writing first draft, Damtew.D.; wrote and edited the review, Damtew.D., A.D., M.S.R. and M.K.L.; reveal, Damtew.D.; control, Damtew.D., A.D., M.S.R. and M.K.L. All authors have read and agreed to the published manuscript.

Funding: This study received no external funding.

Institutional Review Board Statement: Not applicable.

Informed Consent Statement: Not applicable.

Statement of Data Availability: The data used in this study can be obtained from the authors upon reasonable request.

Acknowledgments: The authors would like to thank the University of Rostock for their willingness to fund this publication under the Open Access Publication funding program.

Conflicts of Interest: The authors declare no conflicts of interest or financial conflicts to disclose.

References

1. EPA, "The Effect of Climate Change on Water Resources and Programs," *Watershed Acad. Web*, no. U.S.Environmental Protection Agency, 2012.
2. IPCC-TGICA, "General Guidelines on the Use of Scenario Data for climate impact and adaptation assessment," *Finnish Environ. Inst.*, vol. 312, no. June, p. 66, 2007.
3. IPCC, "Climate Change 2001: The Scientific Basis. Contribution of Working Group I to the Third Assessment Report of the Intergovernmental Panel on Climate Change," 2001.
4. IPCC, "Intergovernmental Panel on Climate Change Climate Change 2007 : Impacts , Adaptation and Vulnerability Working Group II Contribution to the Intergovernmental Panel on Climate Change Fourth Assessment Report Summary for Policymakers," no. 2300, 2007.
5. IPCC-TGICA, "General Guidelines on the Use of Scenario Data for climate impact and adaptation assessment," *Finnish Environ. Inst.*, vol. 312, no. June, p. 66, 2007, [Online]. Available: http://www.citeulike.org/group/14742/article/8861417
6. H. J. Beker, "Evaluation of Surface Water Resource Availability Under Changing Climate Condition in The Erer-Mojo River Subbasin, Wabe-Shebele Basin.," Arba Minch University, Ethiopia, 2018.
7. P. Mukheibir, "Water access, water scarcity, and climate change," *Environ. Manage.*, vol. 45, no. 5, pp. 1027–1039, 2010, doi: 10.1007/s00267-010-9474-6.
8. IPCC, *Climate Change 2007: The Physical Science Basis. Contribution of Working Group I to the Fourth Assessment Report of the Intergovernmental Panel on Climate Change*. Cambridge University Press, Cambridge, United Kingdom and New York, NY, USA, 996 pp, 2007.
9. R. Kiya, "Impact of Climate Change on Water Resources," *J. Earth Sci. Clim. Change*, vol. 05, no. 03, pp. 1–6, 2014, doi: 10.4172/2157-7617.1000185.
10. S. Chattopadhyay and M. K. Jha, "Climate Change Impact Assessment on Watershed Hydrology: A Comparison of Three Approaches," vol. 7, no. 1, pp. 122–128, 2014, doi: 10.3844/ajeassp.2014.122.128.
11. F. Ayivi and M. K. Jha, "International Soil and Water Conservation Research Estimation of water balance and water yield in the Reedy Fork-Buffalo Creek Watershed in North Carolina using SWAT," *Int. Soil Water Conserv. Res.*, vol. 6, no. 3, pp. 203–

Preprints (www.preprints.org) | NOT PEER-REVIEWED | Posted: 11 July 2022 doi:10.20944/preprints202207.0158.v1

213, 2018, doi: 10.1016/j.iswcr.2018.03.007.
12. G. K. Wedajo, M. K. Muleta, B. Gessesse, and S. A. Koriche, "Spatiotemporal climate and vegetation greenness changes and their nexus for Dhidhessa River Basin, Ethiopia," *Environ. Syst. Res.*, vol. 8, no. 1, 2019, doi: 10.1186/s40068-019-0159-8.
13. MoA, *Agro-Ecological Zones of Ethiopia*. 1998.
14. W. T. Bekele, "Implication of Representative Concentration Pathway's On Arjo-Didessa Catchment, Upper Blue Nile Basin, Using Multiple Climate Models," Arba Minch University, 2017.
15. Endris E, R. P. Anitz, and M. B. U. Atthias, "Assessment of the Performance of CORDEX Regional Climate Models in Simulating East African Rainfall," *J. Clim.*, vol. 26, 2013, doi: 10.1175/JCLI-D-12-00708.1.
16. K. Hailemariam, "Impact of climate change on the water resources of Awash River Basin, Ethiopia," *Clim. Res.*, vol. 12, no. 2-3 SPEC. ISS. 6, pp. 91–96, 1999, doi: 10.3354/cr012091.
17. Y. S. Getahun, "Impact of Climate Change on Hydrology of the Upper Awash River Basin (Ethiopia): Inter-comparison of old SRES and new RCP scenarios," no. April 2015, 2018.
18. M. H. Daba, "Evaluating Potential Impacts of Climate Change on Hydro- meteorological Variables in Upper Blue Nile Basin , Ethiopia A Case Study of Finchaa Sub- basin Evaluating Potential Impacts of Climate Change on Hydro- meteorological Variables in Upper Blue Nile B," vol. 6, no. May 2016, pp. 48–57, 2018.
19. K. Kefeni, B. Mokonnen, and N. Roba, "Evaluation the Performance of Regional Climate Models in Simulating Rainfall Characteristics over Upper Awash Sub-Basin , Ethiopia," vol. 5, no. 1, pp. 134–138, 2020.
20. S. Liersch *et al.*, "Are we using the right fuel to drive hydrological models? A climate impact study in the Upper Blue Nile," *Hydrol. Earth Syst. Sci.*, vol. 22, no. 4, pp. 2163–2185, 2018, doi: 10.5194/hess-22-2163-2018b.
21. R. Leander and T. A. Buishand, "Resampling of regional climate model output for the simulation of extreme river flows," *J. Hydrol.*, vol. 332, no. 3–4, pp. 487–496, 2007, doi: 10.1016/j.jhydrol.2006.08.006.
22. W. Terink, R. T. W. L. Hurkmans, P. J. J. F. Torfs, and R. Uijlenhoet, "Evaluation of a bias correction method applied to downscaled precipitation and temperature reanalysis data for the Rhine basin," *Hydrol. Earth Syst. Sci.*, vol. 14, no. 4, pp. 687–703, 2010, doi: 10.5194/hess-14-687-2010.
23. S. G. Setegn, D. Rayner, A. M. Melesse, B. Dargahi, and R. Srinivasan, "Impact of climate change on the hydroclimatology of Lake Tana Basin, Ethiopia," *Water Resour. Res.*, vol. 47, no. 4, pp. 1–13, 2011, doi: 10.1029/2010WR009248.
24. S. . Neitsch, J. . Arnold, J. . Kiniry, and J. . Williams, "Soil & Water Assessment Tool Theoretical Documentation Version 2009," *Texas Water Resour. Inst.*, pp. 1–647, 2011, doi: 10.1016/j.scitotenv.2015.11.063.
25. D. Moriasi, M. Gitau, N. Pai, and P. Daggupati, *Hydrologic and Water Quality Models: Performance Measures and Evaluation Criteria*, no. December. American Society of Agricultural and Biological Engineers ISSN 2151-0032, 2015. doi: 10.13031/trans.58.10715.
26. Z. Xue-song, H. A. O. Fang-hua, C. Hong-guang, and L. I. Dao-feng, "Application of Swat Model In The Upstream Watershed of the Luohe River," vol. 13, no. 4, pp. 334–339, 2003.
27. S. Liersch *et al.*, "Are we using the right fuel to drive hydrological models ? A climate impact study in the Upper Blue Nile," *Hydrol. Earth Syst. Sci. Discuss*, no. September, pp. 1–34, 2016, doi: 10.5194/hess-2016-422.
28. H. V. Gupta, S. Sorooshian, and P. O. Yapo, "Status of Automatic Calibration for Hydrologic Models: Comparison with Multilevel Expert Calibration," *J. Hydrol. Eng.*, vol. 4, no. 2, pp. 135–143, 1999, doi: 10.1061/(asce)1084-0699(1999)4:2(135).
29. D. N. Moriasi, M. W. Gitau, N. Pai, and P. Daggupati, "Hydrologic and water quality models: Performance measures and evaluation criteria," *Trans. ASABE*, vol. 58, no. 6, pp. 1763–1785, 2015, doi: 10.13031/trans.58.10715.
30. F. Fentaw, A. M. Melesse, D. Hailu, and A. Nigussie, *Precipitation and streamflow variability in Tekeze River basin, Ethiopia*. Elsevier Inc., 2019. doi: 10.1016/B978-0-12-815998-9.00010-5.
31. M. Meena, "Rainfall Statistical Trend and Variability Detection Using Mann- Kendall Test , Sen's Slope and Coefficient of

Variance - A Case Study of Udaipur District (1957-2016),” *Appl. Ecol. Environ. Sci.*, vol. 8, no. 1, pp. 34–37, 2020, doi: 10.12691/aees-8-1-5.

32. S. Yue and C. Wang, “The Mann-Kendall Test Modified by Effective Sample Size to Detect Trend in Serially Correlated Hydrological Series,” *Water Resour. Manag.*, pp. 201–218, 2004.
33. WMO, “World Climate Programme : Analyzing Long Time series of hydrological data with respect to climate variability,” no. WMO/TD-No. 224, 1988.
34. O. Masimba, W. Gumindoga, A. Mhizha, and D. T. Rwasoka, “An assessment of baseline and downscaled projected climate variables in the Upper Manyame sub-catchment of Zimbabwe,” *Phys. Chem. Earth*, 2019, doi: 10.1016/j.pce.2019.07.001.
35. F. W. Zwiers, “Global Increasing Trends in Annual Maximum Daily Precipitation,” *J. Clim.*, vol. 26, no. 2005, pp. 3904–3919, 2012, doi: 10.1175/JCLI-D-12-00502.1.
36. M. Bourqui, T. Mathevet, J. Gailhard, and F. Hendrickx, “Hydrological validation of statistical downscaling methods applied to climate model projections,” *IAHS-AISH Publ.*, vol. 344, no. July, pp. 32–38, 2011.
37. F. Movahedinia, “Assessing hydro-climatic uncertainties on hydropower generation,” pp. 1–50, 2014.
38. K. S. Abdo, B. M. Fiseha, T. H. M. Rientjes, A. S. M. Gieske, and A. T. Haile, “Assessment of climate change impacts on the hydrology of Gilgel Abay catchment in Lake Tana basin, Ethiopia,” *Hydrol. Process.*, vol. 23, no. 26, pp. 3661–3669, 2009, doi: 10.1002/hyp.7363.